First posted online on 27 May 2020 as 10.1242/dmm.043091
Access the most recent version at http://dmm.biologists.org/lookup/doi/10.1242/dmm.043091

The zebrafish as a novel model for the *in vivo* study of *Toxoplasma gondii* replication and interaction with macrophages

Nagisa Yoshida[1,2,3], Marie-Charlotte Domart[4], Christopher J. Peddie[4], Artur Yakimovich[5,6], Maria J. Mazon-Moya[2], Thomas A. Hawkins[7], Lucy Collinson[4], Jason Mercer[5,8], Eva-Maria Frickel[1,8*], Serge Mostowy[2,3*]

[1]Host-*Toxoplasma* Interaction Laboratory, The Francis Crick Institute, 1 Midland Road, London NW1 1BF, UK

[2]Section of Microbiology, MRC Centre for Molecular Bacteriology and Infection, Imperial College London, London SW7 2AZ, UK

[3]Department of Infection Biology, London School of Hygiene & Tropical Medicine, Keppel Street, London WC1E 7HT, UK

[4]Electron Microscopy Science Technology Platform, Francis Crick Institute, 1 Midland Road, London NW1 1BF, UK

[5]MRC-Laboratory for Molecular Cell Biology, University College London, Gower Street, London, WC1E 6BT, UK

[6]Artificial Intelligence for Life Sciences CIC, 40 Gowers Walk, London, E1 8BH, UK

[7]Department of Cell and Developmental Biology, University College London, Gower Street, London, WC1E 6BT, UK

[8]Institute of Microbiology and Infection, School of Biosciences, University of Birmingham, Edgbaston, B15 2TT, UK

*Co-senior, co-corresponding authors

Co-corresponding author contact information:

serge.mostowy@lshtm.ac.uk, e.frickel@bham.ac.uk

Summary statement

We have established a novel zebrafish infection model to investigate *Toxoplasma* replication *in vivo*, and demonstrate a key role for macrophages in parasite control.

Key words: CLEM, *In Vivo*, Macrophages, *Toxoplasma gondii*, Zebrafish

Abstract

Toxoplasma gondii is an obligate intracellular parasite capable of invading any nucleated cell. Three main clonal lineages (type I, II, III) exist and murine models have driven the understanding of general and strain-specific immune mechanisms underlying *Toxoplasma* infection. However, murine models are limited for studying parasite-leukocyte interactions *in vivo*, and discrepancies exist between cellular immune responses observed in mouse versus human cells. Here, we developed a zebrafish infection model to study the innate immune response to *Toxoplasma in vivo*. By infecting the zebrafish hindbrain ventricle, and using high-resolution microscopy techniques coupled with computer vision driven automated image analysis, we reveal that *Toxoplasma* invades brain cells and replicates inside a parasitophorous vacuole to which type I and III parasites recruit host cell mitochondria. We also show that type II and III strains maintain a higher infectious burden than type I strains. To understand how parasites are cleared *in vivo*, we further analyzed *Toxoplasma*-macrophage interactions using time-lapse microscopy and three-dimensional correlative light and electron microscopy (3D CLEM). Time-lapse microscopy revealed that macrophages are recruited to the infection site and play a key role in *Toxoplasma* control. High-resolution 3D CLEM revealed parasitophorous vacuole breakage in brain cells and macrophages *in vivo*, suggesting that cell-intrinsic mechanisms may be used to destroy the intracellular niche of tachyzoites. Together, our results demonstrate *in vivo* control of *Toxoplasma* by macrophages, and highlight the possibility that zebrafish may be further exploited as a novel model system for discoveries within the field of parasite immunity.

Introduction

Toxoplasma gondii is a successful human pathogen that often remains asymptomatic, although complications can arise in the immunocompromised and in neonates if infection is contracted during pregnancy (Pappas *et al.*, 2009). *Toxoplasma* exist as invasive rapidly replicating tachyzoites in intermediate hosts (such as rodents and livestock), and convert into bradyzoite cysts in immune privileged sites and long-lived cells (such as the brain and muscle tissue) during chronic infection (Pittman and Knoll, 2015). Once inside the host cell, parasites reside in a non-fusogenic parasitophorous vacuole (PV) where *Toxoplasma* asexually replicates (Clough and Frickel, 2017). Egress leads to dissemination into neighboring tissues, culminating in systemic infection. Predation of intermediate hosts by the definitive feline host completes the *Toxoplasma* life cycle. Control of infection by the host immune response is thus critical both for host survival and for continued parasite transmission. As a result of its well-understood life cycle, *Toxoplasma* has emerged as a valuable model organism to understand the balance between pathogen survival and innate cellular immune control.

Three clonal lineages of *Toxoplasma* dominate across Europe and South America, namely the type I, II and III strains (Howe and Sibley, 1995). These three closely-related *Toxoplasma* strains have been characterized by the severity of infections they cause in murine models (Gazzinelli *et al.*, 2014). Infection with type I parasites causes acute mouse mortality, whereas infection with type II and type III parasites progresses towards chronic infection (Saeij *et al.*, 2005; Szabo and Finney, 2017). In humans, it is thought that type II strains predominate in Europe, yet strain-dependent differences in

pathogenesis and host responses are poorly understood (Ajzenberg *et al.*, 2002; Ajzenberg *et al.*, 2009).

Innate immune mechanisms against *Toxoplasma* infection have been studied *in vitro* using both murine and human cell lines, and *in vivo* using mice. *In vivo* studies have shown monocytes and neutrophils are recruited to the intestine upon oral infection, and are the major cell types infected with *Toxoplasma* both *in vivo* and *ex vivo* in human peripheral blood (Channon *et al.*, 2000; Gregg *et al.*, 2013; Coombes *et al.*, 2013; Harker *et al.*, 2015). The importance of neutrophils in parasite control *in vivo* is not fully understood, yet neutrophil-specific depletion studies have suggested a minor protective role against *Toxoplasma* (Del Rio *et al.*, 2001; Denkers *et al.*, 2012). In contrast, inflammatory monocytes are the first responders to infection and are crucial for controlling acute *Toxoplasma* infection (Mordue and Sibley, 2003; Robben *et al.*, 2005; Dunay *et al.*, 2008). Pioneering work identified the ability of macrophages to kill *Toxoplasma* (Murray *et al.*, 1979; Murray and Cohn, 1979), by employing both IFN-γ-dependent and -independent mechanisms to control intracellular parasite replication (Sibley *et al.*, 1991; Andrade *et al.*, 2005; Saeij and Frickel, 2017).

While the mouse is a natural intermediate host and remains an important model to understand *Toxoplasma* pathogenesis, differences are emerging between the mouse and human in mechanisms of parasite control (Gazzinelli *et al.*, 2014; Yarovinsky *et al.*, 2008; Haldar *et al.*, 2015; Tosh *et al.*, 2016; Sher *et al.*, 2017; Safronova *et al.*, 2019). Therefore, to complement *in vivo* murine studies, a novel animal model can benefit analysis of *Toxoplasma* control on a cellular and molecular level. Zebrafish are a well-established

model for studying infection and immunity (Renshaw and Trede, 2012; Yoshida *et al.*, 2017; Torraca and Mostowy, 2018; Gomes and Mostowy, 2020). Coupled with their optical accessibility during early development, zebrafish larvae are highly suited for non-invasive study of *Toxoplasma* infection and host response in real-time *in vivo* (Torraca and Mostowy, 2018; Gomes and Mostowy, 2020).

Here, we developed a zebrafish infection model to study strain-dependent infectivity and leukocyte response to *Toxoplasma* infection in the hindbrain. We show that *Toxoplasma* invade and replicate inside brain cells including post-mitotic neurons, and that type II (Pru) and III (CEP) parasites maintain a higher infectious burden than type I (RH) parasites. We also demonstrate that macrophages are crucial in the clearance of viable parasites, and use high-resolution three-dimensional correlative light and electron microscopy (3D CLEM) techniques to reveal a discontinuous PV in brain cells and macrophages. Our zebrafish infection model can therefore be used as a novel platform to enable unprecedented discoveries in strain-dependent parasite immunity.

Results

Intracellular *Toxoplasma* replicate in the zebrafish hindbrain ventricle

To develop a *Toxoplasma*-zebrafish infection model, we tested if tachyzoites could replicate in zebrafish larvae. We first used *Toxoplasma* type I (RH) strain, since it is known to grow faster *in vitro* and survive longer extracellularly than type II (Pru) and type III (CEP) strains (Saeij *et al.*, 2005; Khan *et al.*, 2009; Yang *et al.*, 2013). We injected zebrafish larvae 3 days post-fertilization (dpf) in the hindbrain ventricle (HBV) with ~5x10^3 type I strain tachyzoites expressing GFP and followed infection for 24 hours at 33°C (Fig. S1A). We observed parasite replication *in vivo* using time-lapse widefield fluorescent microscopy (Fig. S1B, Movie 1). Consistent with this, confocal microscopy showed that the percentage of vacuoles containing two or more tachyzoites significantly increased with time (Fig. 1A and B). To visualize PV formation around the replicating parasites, infected larvae were fixed and stained for granule antigen 2 (GRA2), a dense granule protein that accumulates in the PV lumen (Mercier *et al.*, 2002). Here, GRA2 accumulated around single and replicating parasites, highlighting PV formation *in vivo* (Fig. 1C).

To investigate parasite morphology and location at 6 hours post-infection (hpi), 3D CLEM using serial blockface scanning electron microscopy (SBF SEM) was performed on the HBV of infected zebrafish. We observed 39 parasites (from n=2 larvae) located inside cells of the zebrafish hindbrain which all displayed host mitochondrial association (Fig. 2A, Fig. S2, Movie 2, Fig. 6), a hallmark of intracellular type I parasites previously described in mouse and human cells (Pernas *et al.*, 2014). Moreover, tachyzoites could be

observed as singlets, replicating doublets (thus joined together), or fully replicated doublets (two tachyzoites not joined together) (Fig. 2A, Fig. S2, Movie 2).

To characterize the specific cell type within which type I parasites reside and replicate in the zebrafish hindbrain, we used Tg(*elavl3*:*GCaMP6s*)^{jf4} transgenic larvae. The elavl3 promoter drives expression in post-mitotic CNS cells fated to become neurons (Park *et al.*, 2000). Embryos harboring this transgene were infected with type I-Tomato parasites (Fig. 2B, Movie 3). In agreement with 3D CLEM data showing that tachyzoites reside within brain cells, infection of *elavl3*:*GCaMP6s* transgenic larvae revealed that ~1/3 of tachyzoites (5/14 and 8/25 from n=2 larvae) reside within GFP$^+$ cells at 4 hpi. Collectively, these results show type I *Toxoplasma* tachyzoites can invade zebrafish cells and replicate *in vivo*, and that tachyzoites favor brain cells over myeloid cells in the zebrafish hindbrain.

Type II and III parasites are more efficient than type I parasites at establishing infection *in vivo*

To determine if parasite strain can affect parasite burden and host response in our zebrafish model, we infected larvae with ~5x10^3 type I, type II or type III *Toxoplasma*-GFP (Fig. S3A). In all cases, infected larvae showed 100% survival and no adverse effects up to 48 hpi (Fig. S3B). To quantify parasite burden in a high-throughput manner, we optimized an automated quantification pipeline using ZedMate (Yakimovich *et al.*, 2019) for the different strain types at 6 and 24 hpi. Strikingly, type II and III parasite burden was ~3x higher than type I parasite burden at 6 hpi (Fig. 3A and B, Fig. S3C).

Analysis by fluorescent stereomicroscopy showed, from initial parasite input of ~5x10^3 tachyzoites (Fig. S3A), parasite burden was reduced ~95% by 6 hpi, suggesting ~5% of parasites (~250 tachyzoites, Fig. 3B, Fig. S3C) successfully invade zebrafish cells and establish infection. Once established at 6 hpi, all 3 strain types persisted equally and decreased by ~20% between 6 and 24 hpi.

To test if host mitochondrial association was observed across the three strain types, we stained host mitochondria in the HBV of infected zebrafish larvae. In agreement with *in vitro* observations (Pernas *et al.*, 2014), ~82% and ~70% of type I and type III parasites, respectively, showed clear host mitochondrial association, while only ~20% of type II parasites showed clear host mitochondria association (Fig. 3C and D). These results demonstrate that strain type-dependent host mitochondrial association characteristics are conserved in zebrafish *in vivo*.

Macrophage and neutrophil response to parasite infection *in vivo*

To analyze *Toxoplasma*-macrophage interactions over time, 3 dpf transgenic larvae possessing red macrophages Tg(*mpeg1*:*Gal4-FF*)^{gl25}/Tg(*UAS-E1b*:*nfsB*.mCherry)^{c264} (herein referred to as *mpeg1*:*G/U*:mCherry), were infected with type I, II or III *Toxoplasma*-GFP, and macrophage recruitment was quantified by fluorescent stereomicroscopy. As compared to mock injection, the number of macrophages recruited to the infection site was significantly increased (~1.5 fold) for all three strain types at both 6 and 24 hpi (Fig. 4A and B).

To analyze *Toxoplasma*-neutrophil interactions over time, 3 dpf transgenic larvae possessing red neutrophils Tg(*lyz*:dsRed)^{nz50} (herein referred to as *lyz*:dsRed), were infected with type I, II or III *Toxoplasma*-GFP, and neutrophil recruitment was quantified by fluorescent stereomicroscopy. Here, the number of neutrophils recruited to the infection site was significantly increased (~3 fold) as compared to mock injection for all three strain types at 6 hpi (Fig. 4C and D). In contrast to macrophages, which remained at the infection site by 24 hpi, the number of neutrophils recruited to the infection site (for all three strain types) decreased significantly, reaching basal levels by 24 hpi.

Macrophages control parasite burden *in vivo*

To analyze the interactions between type I *Toxoplasma* and macrophages in depth, we imaged infected *mpeg1*:*G/U*:mCherry larvae with *Toxoplasma*-GFP at 6 hpi by 3D CLEM. Of the 18 tachyzoites found inside macrophages (from n=3 larvae), seven were intact parasites that had actively invaded macrophages, as identified by host mitochondrial association to the membrane surrounding the parasites (Fig. S4). Six of the seven intact tachyzoites were single tachyzoites inside PVs. This suggests that macrophages may prevent parasite replication. Conversely, a single event captured by 3D CLEM showed *Toxoplasma* replication within a zebrafish macrophage, as judged by host mitochondrial association to the vacuolar membrane and the presence of two replicating tachyzoites (still joined together), with one of the replicating tachyzoites harboring two nuclei (Fig. S5A and B, Movie 4). To follow the fate of type I parasites engulfed by

macrophages in real-time, *mpeg1*:*G/U*:mCherry larvae infected with *Toxoplasma*-GFP were imaged by time-lapse confocal microscopy. Here, we captured the movement of macrophages in the hindbrain harboring type I parasites that had been actively invaded, as identified by host mitochondrial association (Fig. S5C), suggesting that in some cases macrophages may facilitate parasite movement in the brain tissue. However, we also observed parasite engulfment by macrophages followed by loss of GFP fluorescence, suggesting active parasite degradation (Fig. 5A, Movie 5). Consistent with this, 3D CLEM showed parasite degradation inside macrophages, as identified by fragmentation of tachyzoite organelles (Fig. 5B, Fig. S6).

To investigate the structure of the PV surrounding tachyzoites inside brain cells and macrophages in the hindbrain, we imaged *mpeg1*:*G/U*:mCherry larvae infected with *Toxoplasma*-GFP using high-resolution correlative serial section transmission electron microscopy (ssTEM) and focused ion beam scanning electron microscopy (FIB SEM). At 6 hpi, ssTEM revealed gaps in the PV around type I tachyzoites in brain cells (Fig. 6, Movie 6). Consistent with this, and reports of vacuole breakage in human macrophages (Fisch *et al.*, 2019), FIB SEM also captured incomplete vacuole membranes around type I tachyzoites within a macrophage (Fig. 7, Movie 7). Together, ssTEM and FIB SEM demonstrate that cell-intrinsic host immune pathways may be activated within both zebrafish brain cells and macrophages in order to control *Toxoplasma* infection.

To test the role of macrophages in *Toxoplasma* infection at the whole organism level, we used the transgenic line Tg(*mpeg1*:*Gal4-FF)*^{gl25}/Tg(*UAS-E1b*:*nfsB*.mCherry)^{c264} which enables the specific ablation of macrophages

upon metronidazole treatment (Fig. S7A and B). In the absence of macrophages, infected larvae showed 100% survival (Fig. S7C). However, upon infection of ~5x10^3 type I tachyzoites, parasite burden was significantly increased in the absence of macrophages at both 6 and 24 hpi, suggesting that macrophages are responsible for parasite clearance *in vivo* (Fig. 8A and B, Fig. S7D and E). Similarly, a significant increase in parasite burden in macrophage-ablated larvae (as compared to control larvae) was observed upon infection of ~5x10^3 type II and III tachyzoites (Fig. S7F and G). To analyze the viability of parasites that are cleared by macrophages, we performed pixel volume quantification and show that control and Mtz-treated larvae are comprised of equally replicating *Toxoplasma* tachyzoites (% of total vacuoles counted in the HBV; Fig. 8C). These data suggest that macrophages have a dominant role in clearing healthy, viable parasites rather than supporting their replicative niche.

Discussion

Zebrafish infection models for studying eukaryotic parasites are beginning to emerge (Gomes and Mostowy, 2020; Doro *et al.*, 2019). In this study, we established a novel *Toxoplasma* infection model using zebrafish larvae to explore host-parasite interaction *in vivo* in the hindbrain. We found that the three main clonal lineages of *Toxoplasma* are able to establish infection in the zebrafish hindbrain and replicate within their PV, and reveal that macrophages are key in controlling viable parasites *in vivo*. Using the type I strain we showed that *Toxoplasma* invade zebrafish brain cells (including

post-mitotic cells fated to become neurons, expressing GCaMP6s driven by the *elavl3* promoter). Additionally, using state of the art electron microscopy techniques, we observed vacuole breakage around tachyzoites in both zebrafish brain cells and macrophages *in vivo*.

Using time-lapse confocal microscopy and 3D CLEM, we visualized single and replicating type I tachyzoites in the zebrafish HBV exhibiting host mitochondrial association. The relatively slow replication cycle of *Toxoplasma* observed in tissue culture cells *in vitro* (>6 h) is consistent with that observed in the zebrafish HBV. GRA2 staining and 3D CLEM of replicating tachyzoites strongly suggests the formation of a PV. This is indicative of normal type I parasite behavior, as demonstrated *in vitro* using tissue culture cells and *in vivo* using other animal models (Black and Boothroyd, 2000).

The zebrafish HBV is well established to investigate host response to infection (Yoshida *et al.*, 2017; Torraca and Mostowy, 2018; Gomes and Mostowy, 2020). We did not observe *Toxoplasma* dissemination from the HBV, and this allowed us to monitor leukocyte-parasite interactions within a localized area. Here, type II and III strains were more efficient than type I strains at maintaining a higher infectious burden. This suggests that type II and III strains may be more efficient at invading non-phagocytic cell types found in the HBV and/or evading clearance by host cells. Together with 3D CLEM and confocal microscopy, we conclude that *Toxoplasma* can invade non-phagocytic cells (with ~1/3 of parasites within post-mitotic neurons) in the HBV of zebrafish larvae. Although mortality was not observed in our 24 h *Toxoplasma* infection model, it will be of great interest to explore the long-

term consequences of *Toxoplasma* infection on parasite dissemination and zebrafish survival.

Both live-cell imaging and 3D CLEM showed type I parasite uptake and clearance by macrophages. In all cases of macrophage-parasite interaction captured by 3D CLEM, macrophages retained their fluorescence during *Toxoplasma* infection and had intact nuclei and mitochondria, indicative of a healthy host cell. Conversely, phagocytosed tachyzoites (i.e. those that had not entered by active invasion) exhibited no host mitochondrial association, which suggests no PV formation, and showed loss of organelle integrity. Our evidence obtained from time-lapse microscopy, 3D CLEM and macrophage ablation experiments highlight that active parasite clearance by zebrafish macrophages *in vivo* occurs within the first 6 hpi. Using ssTEM and FIB SEM, we observed incomplete PV membrane in zebrafish brain cells and macrophages. PV breakage has been observed *in vitro* after IFN-γ-stimulation of murine cells and human macrophages, and is thought to be part of the cell-intrinsic host defense mechanism against *Toxoplasma* tachyzoites (Martens *et al.*, 2005; Zhao *et al.*, 2008; Yamamoto *et al.*, 2012; Selleck *et al.*, 2015; Fisch *et al.*, 2019). Zebrafish possess an orthologue of IFN-γ together with a related gene (IFN-γ-rel), and studies have suggested zfIFN-γ expression is associated with host protection against bacterial infection, while IFN-γ-rel expression is associated with host protection against viral challenge (Igawa *et al.*, 2006; Lopez-Munoz *et al.*, 2009; Sieger *et al.*, 2009; Lopez-Munoz *et al.*, 2011; Yoon *et al.*, 2016). Therefore, future work using our zebrafish infection model could explore the precise anti-parasitic mechanisms (including the role

of IFN-γ and IFN-γ-rel) employed by brain cells and macrophages during *Toxoplasma* infection.

In murine *in vivo* models, various leukocytes have been implicated in trafficking *Toxoplasma* from the site of infection. Examples include infected neutrophils that pass from the intestine to the lumen (Coombes *et al.*, 2013), as well as infected macrophages and dendritic cells that pass the blood brain barrier (Courret *et al.*, 2006). It is intriguing therefore to note that our study using time-lapse microscopy showed parasite-infected macrophages moving through brain tissue for possible parasite transport (Fig. S5C). Analysis of our 3D CLEM data also identified an actively replicating type I parasite inside a macrophage exhibiting association of host mitochondria with the PV (Fig. S5A-B). This observation is reminiscent of parasite replication “hot spots” described *in vivo* in the murine intestinal villi (Coombes *et al.*, 2013). Injection of tachyzoites directly into the hindbrain of zebrafish is likely to promote *Toxoplasma* infection of neurons (its favored long-term niche; (Ferguson and Hutchison, 1987; Cabral *et al.*, 2016)), and may explain the lack of parasite dissemination by macrophages observed in our model. Overall, it is remarkable that zebrafish macrophages during *Toxoplasma* infection *in vivo* have the capacity to phenocopy known behavior exhibited by murine macrophages during *Toxoplasma* infection *in vivo*. This is the case for both the type of event observed (e.g. parasite killing, trafficking, sustaining replication), and their approximate *in vivo* frequency.

In summary, we have established a novel animal model for studying the *in vivo* innate immune response to *Toxoplasma* infection, and for comparing host response to the three main *Toxoplasma* strain types *in vivo*.

We also demonstrate a dominant role for macrophages in parasite clearance. Having established a zebrafish model of *Toxoplasma* infection, we have revealed a unique *in vivo* infection platform for CRISPR targeting and high-throughput drug screens that, together with time-lapse microscopy, can be used to identify determinants underlying *Toxoplasma* infection control.

Material and methods

Ethics statement

Animal experiments were performed according to the Animals (Scientific Procedures) Act 1986 and approved by the Home Office (Project licenses: PPL P84A89400 and P4E664E3C). All experiments were conducted up to 5 days post-fertilization.

Zebrafish husbandry and maintenance

Fish were reared and maintained at 28.5°C on a 14 h light, 10 h dark cycle. Embryos obtained by natural spawning were maintained in 0.5x E2 media supplemented with 0.3 μg/ml methylene blue. Larvae were anesthetized with 20 μg/ml tricaine (Sigma-Aldrich) during the injection procedures and for live *in vivo* imaging. All experiments were carried out on TraNac background (Krauss *et al.*, 2013) larvae to minimize obstruction of fluorescence signal by pigmentation leading to misrepresentation in parasite dose quantification.

Parasite culture, preparation and infection

Toxoplasma (RH/Pru/CEP) expressing GFP/luciferase or Tomato was maintained *in vitro* by serial passage on human foreskin fibroblasts (HFFs) cultures (ATCC, CVCL_3285). Cultures were grown in DMEM high glucose (Life Technologies) supplemented with 10% FBS (Life Technologies) at 37°C in 5% CO_2. Parasites were prepared from 25G followed by 27G syringe-lysed HFF cultures in 10% FBS. Excess HFF material removed by centrifugation for 10 min at 50 x g. After washing with PBS, *Toxoplasma* tachyzoites were resuspended at $2x10^6$ tachyzoites/µl in PBS. During injection, tachyzoites were maintained at room temperature and passed through a 29G myjector syringe (Terumo) to dissociate clumps and homogenize the suspension. Control infections were carried out using uninfected HFF cultures prepared as described above. 3 dpf larvae were anesthetized and injected with ~2 nl of parasite suspension into the HBV. HBV injections were carried out as previously described (Mazon Moya *et al.*, 2017). Larvae are optimally maintained at 28.5°C, but develop normally between 23-33°C (Westerfield, 2007). *Toxoplasma* invades and replicates at a minimum of 33°C. Infected larvae were therefore transferred into media pre-warmed to 33°C to ensure normal zebrafish development and parasite replication (Fig. S1A). Progress of infection was monitored by fluorescent stereomicroscopy (Leica M205FA, Leica Microsystems).

Quantification of parasite dose and burden

For parasite dose quantification Z-stacks of the infected hindbrain were taken within 5-10 min using the Leica M205FA fluorescent stereomicroscope on a

130x magnification using a 1x objective. Images were analyzed using the particle analysis function in Fiji software (Schindelin *et al.*, 2012). For manual quantification of parasite burden, Z-stacks were taken using the Leica M205FA. GFP-positive punctae were quantified using the multi-point tool in Fiji software. Computer vision driven automated parasite burden quantifications were carried out using the ZedMate plugin in Fiji software to corroborate manual quantifications (Yakimovich *et al.*, 2019). Pixel volume quantifications were carried out by 3D projecting confocal Z-stacks and using the 3D objects counter tool in Fiji (Movie 8). For Movie 8 scale was increased from 124 x 165 pixels (11 pixels = 4.8 μm) to 1240 x 1650 pixels for clarity.

Live imaging, image processing and analysis

Live *in vivo* imaging was performed on anesthetized larvae immobilized in 1% low melting-point agarose in 35 mm glass-bottomed dishes (MatTek Corp.). Widefield microscopy was performed using a 40x objective. Z-stacks were acquired at 10 minute intervals. 60 Z-slices were taken at 2 μm sections. Post-acquisition, scale was increased from 155 x 155 pixels (100.75 x 100.75 μm) to 1000 x 1000 pixels, and further cropped to a final size of 204 x 204 pixels around the region of interest. Confocal microscopy was performed using the Zeiss Invert LSM 710 (Carl Zeiss AG) and the LSM 880 (Carl Zeiss AG) using a 40x and 63x objective. Z-stacks were acquired at 8 minute intervals. 60 Z-slices were taken at 0.9 μm sections per larva. For all time-lapse acquisitions, larvae were maintained at 33°C. For mitochondria staining, larvae were injected with 1 nl MitoTracker® DeepRed (250 μM, Life Technologies) 40 min prior to embedding for live confocal microscopy. For

characterization of the cell type that *Toxoplasma* tachyzoites are invading, the Tg(*elavl3*:*GCaMP6s*)^{jf4} transgenic line was used. This particular transgenic line employs an enhanced GFP protein variant fused to calcium binding proteins to read out neuronal calcium flux (Vladimirov *et al.,* 2014); however, we did not employ the calcium sensitivity functionality for our experiments: it was used purely to identify neurons. For confocal microscopy of Tg(*elavl3*:*GCaMP6s*)^{jf4} larvae LSM 880 (Carl Zeiss AG) was used with the 63x objective. For Movie 3 a confocal Z-stack of 33 Z-slices (Z=0.43 μm) was acquired. Post acquisition, scale was increased from 1232 x 1232 pixels (104.84 x 104.84 μm) to 2000 x 2000 pixels. For Fig. 2B a Z-stack of 85 slices (covering 14.525 μm) was acquired using the AiryScan super-resolution (SR) mode and processed using AiryScan processing tool in Zen Blue (Carl Zeiss AG).

Wholemount immunohistochemistry

Euthanized larvae were fixed overnight at 4°C in 4% paraformaldehyde supplemented with 0.4% Triton X-100 and washed in PBS, 0.4% Triton X-100 before staining. Briefly, after a 20 min wash in PBS 1% Triton X-100, larvae were incubated overnight at 4°C in blocking solution: PBS, supplemented with 10% FBS, 1% DMSO and 0.1% Tween 20. Primary antibodies diluted 1:1000 in blocking solution were applied overnight at 4°C. Larvae were washed 4x15 min with PBS supplemented with 0.1% Tween 20. Secondary antibodies diluted 1:500 in blocking solution were applied overnight at 4°C. Larvae were washed 4x15 min with PBS supplemented with 0.1% Tween 20. Hoechst 33342 staining of larvae was carried out at room temperature for 10 min,

followed by 3x10 min washes with PBS, 0.1% Tween 20. Larvae were then cleared by sequential incubation in increasing glycerol concentrations: 15% glycerol for 1 hr at room temperature, 30% glycerol overnight at 4°C, 60% glycerol overnight at 4°C, 80% glycerol overnight at 4°C before imaging by AiryScan confocal microscopy (Zeiss LSM 880). Z-stacks were obtained at intervals of 0.46 μm using the AiryScan super-resolution (SR) mode.

Antibodies

Primary antibodies used were mouse α-GRA2 (#BIO.018.5, BIOTEM), kind gift of Moritz Treeck, The Francis Crick Institute, UK. Secondary antibodies used were goat α-mouse AF647 (A-21245, Invitrogen).

Three-dimensional correlative light and electron microscopy (3D CLEM)

Euthanized larvae were fixed overnight at 4°C in 4% formaldehyde (Taab Laboratories Equipment Ltd.). Hoechst 33342 staining of larvae was carried out at room temperature for 10 min without permeabilization and larvae were subsequently washed 3x10 min with 0.1 M phosphate buffer (PB). Larvae were embedded in 3% low-melt agarose in 35 mm glass-bottomed dishes. Larvae were covered in 0.1 M PB for high-resolution confocal microscopy (Zeiss LSM 710). Larvae were maintained in 1% formaldehyde in 0.1 M PB until further processing. The embedded larvae were sectioned using a Leica VT1000 S vibrating blade microtome (Leica Biosystems). 50 μm sections were collected and stored in 0.1 M PB in a 24-well glass-bottomed plate (MatTek Corp.). The sections were imaged again using a Zeiss Invert 710 LSM confocal (Carl Zeiss AG) and a 20x Ph2 objective. The sections

containing *Toxoplasma* were then processed following the method of the National Centre for Microscopy and Imaging Research (Deerink *et al.*, 2010). In brief they were post-fixed in 2.5% (v/v) gluteraldehyde/4% (v/v) formaldehyde in 0.1 M PB for 30 min at room temperature, stained in 2% osmium tetroxide/1.5% potassium ferricyanide for 1 h on ice, incubated in 1% w/v thiocarbohydrazide for 20 min before a second staining with 2% osmium tetroxide, and incubation overnight in 1% aqueous uranyl acetate at 4˚C. Sections were stained with Walton's lead aspartate for 30 min at 60°C and dehydrated stepwise through an ethanol series on ice, incubated in a 1:1 propylene oxide/Durcupan resin mixture and embedded in Durcupan ACM® resin according to the manufacturer's instructions (Sigma-Aldrich). Blocks were trimmed to a small trapezoid, excised from the resin block and attached to a SBF SEM specimen pin using conductive epoxy resin (Circuitworks CW2400).

1) Serial block face scanning electron microscopy (SBF SEM)

Prior to commencement of a SBF SEM imaging run, the sample was coated with a 2 nm layer of platinum to further enhance conductivity using a Q150R S sputter coater (Quorum Technologies Ltd.). SBF SEM data was collected using a 3View2XP (Gatan Inc.) attached to a Sigma VP SEM (Zeiss). Inverted backscattered electron images were acquired through the entire extent of the region of interest. For each 50 nm slice, a low-resolution overview image (pixel size of ~50 nm using a 1.5 μs dwell time) and several high-resolution images of the different regions of interest (indicated magnification ~5000x, pixel size of 6-7 nm using a 1.5 μs dwell time) were acquired. The overview image was used to relocate the region of interest

defined by the confocal images of the sections. The SEM was operated in variable pressure mode at 5 pascals. The 30 μm aperture was used, at an accelerating voltage of 2 kV. Typically, between 300 and 1000 slices were necessary for an entire region of interest. As data was collected in variable pressure mode, only minor adjustments in image alignment were needed, particularly where the field of view was altered in order to track the cell of interest.

2) Serial section transmission electron microscopy (ssTEM)

Prior to ssTEM, the sample was imaged by SBF SEM using low-resolution overview images (100 nm slices, 2 kV, pixel size of 33 nm, 2 μs dwell time, high vacuum with focal charge compensation on at 50%) to relocate the region of interest defined by the confocal images. After SBF SEM, the sample was serial sectioned using a UC7 ultramicrotome (Leica Microsystems) and consecutive 70 nm sections were picked up on Formvar-coated 2 mm slot copper grids (Gilder Grids Ltd.). 143 consecutive sections containing 11 *Toxoplasma* were viewed at 440x, 890x and 6800x (plus some selected areas at 18500x) using a 120 kV Tecnai G2 Spirit transmission electron microscope (Thermo Fisher Scientific) and images were captured using a OneView UltraScan® 4000 camera and GMS3 software (Gatan Inc.). The 3 *Toxoplasma* shown in Fig. 6 were imaged in their full volume (~75 sections).

After sectioning for ssTEM, the sample was imaged again in the SBF SEM at low and high-resolution (pixel size of 35 nm and 6 nm, 50 nm slices, 2 kV, 2 μs dwell time, high vacuum with focal charge compensation on at 50%), until the macrophage to be imaged by FIB SEM appeared.

All the ssTEM and SBF SEM images were converted to tiff in Digital Micrograph or GMS3 (Gatan Inc.), and tiff stacks were automatically aligned using TrakEM2, a Fiji framework plug-in (Cardona *et al.*, 2012). For ssTEM stacks of images, misaligned images were in addition manually aligned to the neighboring sections. Manual segmentations were done in TrakEM2. For Fig. 2A and 6A, labels were exported as tiff for visualization in 3D in ClearVolume, a Fiji plug-in (Royer *et al.*, 2015). For Fig. S5B, they were exported as Amira labels for visualization in 3D in Amira Software (Thermo Fisher Scientific).

3) Focused ion beam scanning electron microscopy (FIB SEM)

FIB SEM data was collected using a Crossbeam 540 FIB SEM with Atlas 5 for 3-dimensional tomography acquisition (Zeiss, Cambridge). After image acquisition for SBF SEM and ssTEM was completed, the sample was further sputter coated with a 10 nm layer of platinum.

The region of interest was relocated by briefly imaging through the platinum coating at an accelerating voltage of 20 kV and correlating to previously acquired SBF SEM and fluorescence microscopy images. The final ROI and milling orientation were targeted in order to preserve the majority of the sample whilst enclosing the entire cell of interest. On completion of preparation for milling and tracking, images were acquired at 5 nm isotropic resolution throughout the region of interest, using a 4.2 μs dwell time. During acquisition the SEM was operated at an accelerating voltage of 1.5 kV with 1.5 nA current. The EsB detector was used with a grid voltage of 1,200 V. Ion beam milling was performed at an accelerating voltage of 30 kV and current of 700 pA.

The final dataset was acquired in two sessions; in order to correct for uneven milled slice thickness in the initial phase of the second session, the first 100 slices were aligned and interpolated to output a per-slice thickness of 5 nm (Atlas 5), prior to reinsertion into the dataset of approximately 24.1 μm x 17.8 μm x 20.2 μm (8,651 μm^3).

After initial registration (template matching by normalized cross correlation; Fiji, https://sites.google.com/site/qingzongtseng/template-matching-ij-plugin), the images were batch processed to suppress noise, and enhance sharpness and contrast (i. gaussian blur 0.8 pixel radius; ii. smart sharpening with highlights suppressed: radius 10 pixels, strength 60%, then radius 1.2 pixels, strength 150%; iii. application of a medium contrast curve; iv. 8-bit greyscale conversion; Adobe Photoshop 2020). Finally, to fine tune image registration, the alignment to median smoothed template method was applied (AMST; (Hennies *et al.*, 2020). Subregions comprising the macrophage, and individual *Toxoplasma* were then cropped out from the final volume.

For Fig. 7A, image stacks from confocal microscopy and FIB SEM were manually aligned to each other using the BigWarp plugin of the Fiji framework (Bogovic *et al.*, 2016), with the FIB SEM stack set as 'target' and the confocal stack as 'moving' dataset. 'Landmark mode' was used to add 19 pairs of corresponding points within both datasets throughout the whole volume of the cell. An affine transformation was applied to the confocal dataset.

Movies 2, 6 and 7 were generated in Fiji, Movie 4 in Amira, and all were compressed in Quick Time Pro with the H.264 encoder.

Measurement of leukocyte recruitment to the site of infection

Anesthetized larvae were imaged 0, 6 and 24 hpi by fluorescent stereomicroscopy (Leica M205FA). 15 Z-slices at 8.55 μm intervals covering 128 μm were taken at 130x magnification. Images were further analyzed using Fiji software.

Metronidazole targeted macrophage depletion

For macrophage ablation the nitroreductase/metronidazole ablation system was utilized (Curado *et al.*, 2008). Metronidazole is converted by nitroreductase into a cytotoxic metabolite. Therefore expression of nitroreductase-mCherry (*nfsB.*mCherry) in the macrophage population in the transgenic line Tg(*mpeg1*:*Gal4-FF)*^{gl25}/Tg(*UAS-E1b*:*nfsB*.mCherry)^{c264} allows for the specific ablation of macrophages upon metronidazole treatment. Dechorionated 2 dpf TraNac-Tg(*mpeg1*:*Gal4-FF)*^{gl25}/Tg(*UAS-E1b*:*nfsB*.mCherry)^{c264} larvae were placed in embryo media supplemented with metronidazole (10 mM, Sigma-Aldrich), 1% DMSO. Larvae were then placed in fresh 10 mM metronidazole solution at 33°C post-infection. Control-treated larvae were maintained in embryo media supplemented with 1% DMSO.

Statistical analysis

Significance testing was performed using unpaired t-test, one-way ANOVA, or 2-way ANOVA (repeated measures with Sidak's/Tukey's multiple comparisons test). For data that does not conform to the assumptions of

parametric statistics, Chi-square or Kruskal-Wallis (with Dunn's multiple comparisons) tests were used. The level of significance is shown as ns, $p>0.05$; *, $p \leq 0.05$; **, $p \leq 0.01$; ***, $p \leq 0.001$.

Acknowledgements. We thank Vincenzo Torraca, Gina Duggan, Margarida Castro Gomes, Joseph Wright and Barbara Clough for scientific discussions. We thank Moritz Treeck for providing the α-GRA2 antibody. We thank Damian Rivett for advice on statistical analysis. We thank Isaac Bianco and the Bianco lab (CDB; UCL) for providing Tg*(elavl3:GCaMP6s)*^{jf4} embryos.

Financial support. NY was supported by a shared Crick-Imperial PhD studentship. This work was supported by the Francis Crick Institute, which receives its core funding from Cancer Research UK (FC001999 to LC, FC001076 to EMF), the UK Medical Research Council (FC001999 to LC, FC001076 to EMF), and the Wellcome Trust (FC001999 to LC, FC001076 to EMF). EMF was supported by a Wellcome Trust Career Development Fellowship (091664/B/10/Z). Research in the Mostowy laboratory is supported by a European Research Council Consolidator Grant (772853 - ENTRAPMENT), Wellcome Trust Senior Research Fellowship (206444/Z/17/Z), Wellcome Trust Research Career Development Fellowship (WT097411MA), and the Lister Institute of Preventive Medicine. Research in the Hawkins laboratory is supported (with TH as Co-I) by a Biotechnology and Biological Sciences Research Council grant (BB/T001844/1) held by Jason Rihel (UCL).

Author Contributions

NY conducted all experiments with the exception of the electron microscopy, MCD conducted all sample preparation, imaging and image analysis for SBF SEM and ssTEM, CJP conducted imaging and image analysis for FIB SEM, MJM initiated the infection model, AY and JM enabled automated image analysis, TAH and LC provided electron microscopy expertise, EMF and SM supervised the study, NY, MCD, EMF and SM wrote the manuscript and all authors provided input.

Potential conflicts of interest. All authors: No reported conflicts of interest

References

Ajzenberg, D., Cogne, N., Paris, L., Bessieres, M. H., Thulliez, P., Filisetti, D., Pelloux, H., Marty, P., and Darde, M. L. (2002). Genotype of 86 *Toxoplasma gondii* isolates associated with human congenital toxoplasmosis, and correlation with clinical findings, *J Infect Dis*, **186**: 684-9.

Ajzenberg, D., Yera, H., Marty, P., Paris, L., Dalle, F., Menotti, J., Aubert, D., *et al.* (2009). Genotype of 88 *Toxoplasma gondii* isolates associated with toxoplasmosis in immunocompromised patients and correlation with clinical findings, *J Infect Dis*, **199**: 1155-67.

Andrade, R. M., Portillo, J. A. C., Wessendarp, M., and Subauste, C. S. (2005). CD40 signaling in macrophages induces activity against an intracellular pathogen independently of gamma interferon and reactive nitrogen intermediates., *Infect. Immun.*, **73**: 3115-23.

Black, M. W., and Boothroyd, J. C. (2000). Lytic cycle of *Toxoplasma gondii.*, *Microbiol. Mol. Biol. Rev.*, **64**: 607-23.

Bogovic, J. A., Hanslovsky, P., Wong, A., and Saalfeld, S. (2016). Robust registration of calcium images by learned contrast synthesis ISBI: 1123-1126, doi:10.1109/ISBI.2016.7493463 https://arxiv.org/abs/1511.01154

Cabral, C. M., Tuladhar, S., Dietrich, H. K., Nguyen, E., MacDonald, W. R., Trivedi, T., Devineni, A., and Koshy, A. A. (2016). Neurons are the primary target cell for the brain-tropic intracellular parasite *Toxoplasma gondii*, *PLoS Pathog*, **12**: e1005447.

Cardona, A., Saalfeld, S., Schindelin, J., Arganda-Carreras, I., Preibisch, S., Longair, M., Tomancak, P., Hartenstein, V., and Douglas, R. J. (2012). TrakEM2 software for neural circuit reconstruction., *PLoS One*, **7**: e38011.

Channon, J. Y., Seguin, R. M., and Kasper, L. H. (2000). Differential infectivity and division of *Toxoplasma gondii* in human peripheral blood leukocytes., *Infect. Immun.*, **68**: 4822-26.

Clough, B., and Frickel, E. M. (2017). The *Toxoplasma* parasitophorous vacuole: an evolving host-parasite frontier., *Trends Parasitol.*, **33**: 473-88.

Coombes, J. L., Charsar, B. A., Han, S. J., Halkias, J., Chan, S. W., Koshy, A. A., Striepen, B., and Robey, E. A. (2013). Motile invaded neutrophils in the small intestine of *Toxoplasma gondii*-infected mice reveal a potential mechanism for parasite spread, *Proc Natl Acad Sci U S A*, **110**: E1913-22.

Courret, N., Darche, S., Sonigo, P., Milon, G., Buzoni-Gatel, D., and Tardieux, I. (2006). CD11c- and CD11b-expressing mouse leukocytes transport single *Toxoplasma gondii t*achyzoites to the brain, *Blood*, **107**: 309-16.

Curado, S., Stainier, D. Y., and Anderson, R. M. (2008). Nitroreductase-mediated cell/tissue ablation in zebrafish: a spatially and temporally controlled ablation method with applications in developmental and regeneration studies, *Nat Protoc*, **3**: 948-54.

Deerink, T. J., Bushong, E. A., and Ellisman, M. H. (2010). NCMIR methods for 3D EM: A new protocol for preparation for biological specimens for serial blockface scanning electron microscopy. https://ncmir.ucsd.edu/sbem-protocol

Del Rio, L., Bennouna, S., Salinas, J., and Denkers, E. Y. (2001). CXCR2 deficiency confers impaired neutrophil recruitment and increased susceptibility during *Toxoplasma gondii* infection, *J Immunol*, **167**: 6503-9.

Denkers, E. Y., Schneider, A. G., Cohen, S. B., and Butcher, B. A. (2012). Phagocyte responses to protozoan infection and how *Toxoplasma gondii* meets the challenge, *PLoS Pathog*, **8**: e1002794.

Doro, E., Jacobs, S. H., Hammond, F. R., Schipper, H., Pieters, R. P., Carrington, M., Wiegertjes, G. F., and Forlenza, M. (2019). Visualizing trypanosomes in a vertebrate host reveals novel swimming behaviours, adaptations and attachment mechanisms, *Elife*, **8**.

Dunay, I. R., Damatta, R. A., Fux, B., Presti, R., Greco, S., Colonna, M., and Sibley, L. D. (2008). Gr1(+) inflammatory monocytes are required for mucosal resistance to the pathogen *Toxoplasma gondii*., *Immunity*, **29**: 306-17.

Ferguson, D. J., and Hutchison, W. M. (1987). The host-parasite relationship of *Toxoplasma gondii* in the brains of chronically infected mice, *Virchows Arch A Pathol Anat Histopathol*, **411**: 39-43.

Fisch, D., Clough, B., Domart, M. C., Bando, H., Masonou, T., Collinson, L. M., Yamamoto, M., Shenoy, A. R., and Frickel, E. M. (2019). Differential spatiotemporal targeting of *Toxoplasma* and *Salmonella* by GBP1 assembles caspase signalling platforms, *bioRxiv* https://doi.org/10.1101/792804.

Gazzinelli, R. T., Mendonça-Neto, R., Lilue, J., Howard, J., and Sher, A. (2014). Innate resistance against *Toxoplasma gondii*: an evolutionary tale of mice, cats, and men., *Cell Host Microbe*, **15**: 132-38.

Gomes, M. C., and Mostowy, S. (2020). The case for modelling human infection in zebrafish, *Trends Microbiol*, **28**: 10-18.

Gregg, B., Taylor, B. C., John, B., Tait-Wojno, E. D., Girgis, N. M., Miller, N., Wagage, S., Roos, D. S., and Hunter, C. A. (2013). Replication and distribution of *Toxoplasma gondii* in the small intestine after oral infection with tissue cysts., *Infect. Immun.*, **81**: 1635-43.

Haldar, A. K., Foltz, C., Finethy, R., Piro, A. S., Feeley, E. M., Pilla-Moffett, D. M., Komatsu, M., Frickel, E. M., and Coers, J. (2015). Ubiquitin systems mark pathogen-containing vacuoles as targets for host defense by guanylate binding proteins, *Proc Natl Acad Sci U S A*, **112**: E5628-37.

Harker, K. S., Ueno, N., and Lodoen, M. B. (2015). *Toxoplasma gondii* dissemination: a parasite's journey through the infected host., *Parasite Immunol.*, **37**: 141-49.

Hennies, J., Lleti, J. M. S., Schieber, N. L., Templin, R. M., Steyer, A. M., and Schwab, Y. (2020). AMST: alignment to median smoothed template for focused ion beam scanning electron microscopy image stacks, *Sci Rep*, **10**: 2004.

Howe, D. K., and Sibley, L. D. (1995). *Toxoplasma gondii* comprises three clonal lineages: correlation of parasite genotype with human disease, *J Infect Dis*, **172**: 1561-6.

Igawa, D., Sakai, M., and Savan, R. (2006). An unexpected discovery of two interferon gamma-like genes along with interleukin (IL)-22 and -26 from teleost: IL-22 and -26 genes have been described for the first time outside mammals, *Mol Immunol*, **43**: 999-1009.

Khan, A., Behnke, M. S., Dunay, I. R., White, M. W., and Sibley, L. D. (2009). Phenotypic and gene expression changes among clonal type I strains of *Toxoplasma gondii*, *Eukaryot Cell*, **8**: 1828-36.

Krauss, J., Astrinidis, P., Astrinides, P., Frohnhofer, H. G., Walderich, B., and Nusslein-Volhard, C. (2013). transparent, a gene affecting stripe formation in Zebrafish, encodes the mitochondrial protein Mpv17 that is required for iridophore survival, *Biol Open*, **2**: 703-10.

Lopez-Munoz, A., Roca, F. J., Meseguer, J., and Mulero, V. (2009). New insights into the evolution of IFNs: zebrafish group II IFNs induce a rapid and transient expression of IFN-dependent genes and display powerful antiviral activities, *J Immunol*, **182**: 3440-9.

Lopez-Munoz, A., Sepulcre, M. P., Roca, F. J., Figueras, A., Meseguer, J., and Mulero, V. (2011). Evolutionary conserved pro-inflammatory and antigen presentation functions of zebrafish IFNgamma revealed by transcriptomic and functional analysis, *Mol Immunol*, **48**: 1073-83.

Martens, S., Parvanova, I., Zerrahn, J., Griffiths, G., Schell, G., Reichmann, G., and Howard, J. C. (2005). Disruption of *Toxoplasma gondii* parasitophorous vacuoles by the mouse p47-resistance GTPases, *PLoS Pathog*, **1**: e24.

Mazon Moya, M. J., Willis, A. R., Torraca, V., Boucontet, L., Shenoy, A. R., Colucci-Guyon, E., and Mostowy, S. (2017). Septins restrict inflammation and protect zebrafish larvae from *Shigella* infection., *PLoS Pathog.*, **13**: e1006467.

Mercier, C., Dubremetz, J. F., Rauscher, B., Lecordier, L., Sibley, L. D., and Cesbron-Delauw, M. F. (2002). Biogenesis of nanotubular network in *Toxoplasma* parasitophorous vacuole induced by parasite proteins., *Molecular Biology of the Cell*, **13**: 2397-409.

Mordue, D. G., and Sibley, L. D. (2003). A novel population of Gr-1 +-activated macrophages induced during acute toxoplasmosis, *J. Leukoc. Biol.*, **74**: 1015-25.

Murray, H. W., and Cohn, Z. A. (1979). Macrophage oxygen-dependent antimicrobial activity. I. Susceptibility of *Toxoplasma gondii* to oxygen intermediates, *J Exp Med*, **150**: 938-49.

Murray, H. W., Juangbhanich, C. W., Nathan, C. F., and Cohn, Z. A. (1979). Macrophage oxygen-dependent antimicrobial activity. II. The role of oxygen intermediates, *J Exp Med*, **150**: 950-64.

Pappas, G., Roussos, N., and Falagas, M. E. (2009). Toxoplasmosis snapshots: global status of *Toxoplasma gondii* seroprevalence and implications for pregnancy and congenital toxoplasmosis., *Int. J. Parasitol.*, **39**: 1385-94.

Park, H. C., Kim, C. H., Bae, Y. K., Yeo, S. Y., Kim, S. H., Hong, S. K., Shin, J.*, et al.* (2000). Analysis of upstream elements in the HuC promoter leads to the establishment of transgenic zebrafish with fluorescent neurons, *Dev Biol*, **227**: 279-93.

Pernas, L., Adomako-Ankomah, Y., Shastri, A. J., Ewald, S. E., Treeck, M., Boyle, J. P., and Boothroyd, J. C. (2014). *Toxoplasma* effector MAF1 mediates recruitment of host mitochondria and impacts the host response., *PLoS Biol.*, **12**: e1001845.

Pittman, K. J., and Knoll, L. J. (2015). Long-term relationships: the complicated Interplay between the host and the developmental stages of *Toxoplasma gondii* during acute and chronic infections, *Microbiol Mol Bio Rev*: 1-15.

Renshaw, S. A., and Trede, N. S. (2012). A model 450 million years in the making: zebrafish and vertebrate immunity., *Dis Model Mech*, **5**: 38-47.

Robben, P. M., LaRegina, M., Kuziel, W. A., and Sibley, L. D. (2005). Recruitment of Gr-1+ monocytes is essential for control of acute toxoplasmosis., *J Exp Med*, **201**: 1761-69.

Royer, L. A., Weigert, M., Günther, U., Maghelli, N., Jug, F., Sbalzarini, I. F., and Myers, E. W. (2015). ClearVolume: open-source live 3D visualization for light-sheet microscopy., *Nat. Methods*, **12**: 480-81.

Saeij, J. P., Boyle, J. P., and Boothroyd, J. C. (2005). Differences among the three major strains of *Toxoplasma gondii* and their specific interactions with the infected host, *Trends Parasitol*, **21**: 476-81.

Saeij, J. P., and Frickel, E. M. (2017). Exposing *Toxoplasma gondii* hiding inside the vacuole: a role for GBPs, autophagy and host cell death., *Curr. Opin. Microbiol.*, **40**: 72-80.

Safronova, A., Araujo, A., Camanzo, E. T., Moon, T. J., Elliott, M. R., Beiting, D. P., and Yarovinsky, F. (2019). Alarmin S100A11 initiates a chemokine response to the human pathogen *Toxoplasma gondii*, *Nat Immunol*, **20**: 64-72.

Schindelin, J., Arganda-Carreras, I., Frise, E., Kaynig, V., Longair, M., Pietzsch, T., Preibisch, S.*, et al.* (2012). Fiji: an open-source platform for biological-image analysis, *Nat Methods*, **9**: 676-82.

Selleck, E. M., Orchard, R. C., Lassen, K. G., Beatty, W. L., Xavier, R. J., Levine, B., Virgin, H. W., and Sibley, L. D. (2015). A noncanonical autophagy pathway restricts *Toxoplasma gondii* growth in a strain-specific manner in IFN-gamma-activated human cells, *mBio*, **6**: e01157-15.

Sher, A., Tosh, K., and Jankovic, D. (2017). Innate recognition of *Toxoplasma gondii* in humans involves a mechanism distinct from that utilized by rodents., *Cell. Mol. Immunol.*, **14**: 36-42.

Sibley, L. D., Adams, L. B., Fukutomi, Y., and Krahenbuhl, J. L. (1991). Tumor necrosis factor-alpha triggers antitoxoplasmal activity of IFN-gamma primed macrophages., *J Immunol*, **147**: 2340-45.

Sieger, D., Stein, C., Neifer, D., van der Sar, A. M., and Leptin, M. (2009). The role of gamma interferon in innate immunity in the zebrafish embryo, *Dis Model Mech*, **2**: 571-81.

Szabo, E. K., and Finney, C. A. M. (2017). *Toxoplasma gondii*: one organism, multiple models, *Trends Parasitol*, **33**: 113-27.

Torraca, V., and Mostowy, S. (2018). Zebrafish infection: from pathogenesis to cell biology, *Trends Cell Biol.*, **28**: 143-56.

Tosh, K. W., Mittereder, L., Bonne-Annee, S., Hieny, S., Nutman, T. B., Singer, S. M., Sher, A., and Jankovic, D. (2016). The IL-12 response of primary human dendritic cells and monocytes to *Toxoplasma gondii* is stimulated by phagocytosis of live parasites rather than host cell invasion., *J. Immunol.*, **196**: 345-56.

Westerfield, M. 2007. *The zebrafish book. A guide for the laboratory use of zebrafish (Danio rerio)* (University of Oregon Press: Eugene).

Yakimovich, A., Huttunen, M., Samolei, J., Clough, B., Yoshida, N., Mostowy, S., Frickel, E. M., and Mercer, J. (2019). Mimicry embedding for efficient capsule network weights transfer in 3D biomedical micrographs, *bioRxiv* https://doi.org/10.1101/820076.

Yamamoto, M., Okuyama, M., Ma, J. S., Kimura, T., Kamiyama, N., Saiga, H., Ohshima, J.*, et al.* (2012). A cluster of interferon-gamma-inducible p65 GTPases plays a critical role in host defense against *Toxoplasma gondii*, *Immunity*, **37**: 302-13.

Yang, N., Farrell, A., Niedelman, W., Melo, M., Lu, D., Julien, L., Marth, G. T., Gubbels, M. J., and Saeij, J. P. (2013). Genetic basis for phenotypic differences between different *Toxoplasma gondii* type I strains, *BMC Genomics*, **14**: 467.

Yarovinsky, F., Hieny, S., and Sher, A. (2008). Recognition of *Toxoplasma gondii* by TLR11 prevents parasite-induced immunopathology, *J Immunol*, **181**: 8478-84.

Yoon, S., Alnabulsi, A., Wang, T. Y., Lee, P. T., Chen, T. Y., Bird, S., Zou, J., and Secombes, C. J. (2016). Analysis of interferon gamma protein expression in zebrafish (Danio rerio), *Fish Shellfish Immunol*, **57**: 79-86.

Yoshida, N., Frickel, E. M., and Mostowy, S. (2017). Macrophage–microbe interactions: lessons from the zebrafish model, *Front Immunol*, **8**: 508.

Zhao, Z., Fux, B., Goodwin, M., Dunay, I. R., Strong, D., Miller, B. C., Cadwell, K.*, et al.* (2008). Autophagosome-independent essential function for the autophagy protein Atg5 in cellular immunity to intracellular pathogens, *Cell Host Microbe*, **4**: 458-69.

Figures

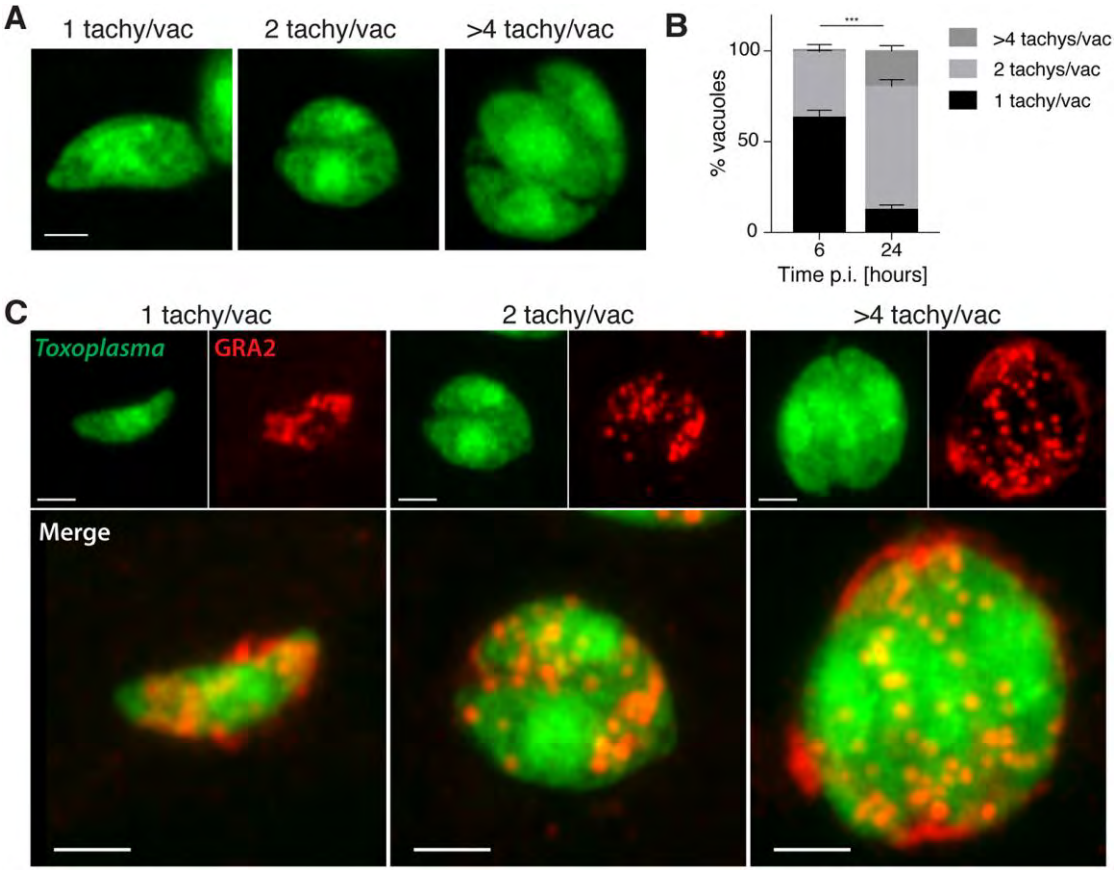

Figure 1. *Toxoplasma gondii* tachyzoites are intracellular and replicate in zebrafish. (A) Representative images from AiryScan confocal imaging of replicating tachyzoites in fixed larvae infected in the HBV with type I *Toxoplasma*-GFP at 6 and 24 hpi. Showing 1, 2 or >4 tachyzoites/vacuole. Scale bar, 5 μm. (B) Pixel volume quantification of individual GFP-positive punctae at 6 and 24 hpi. Significant differences (X^2_2 = 58.5, p≤0.001) were observed between percentage of total vacuoles counted in the HBV that are 1 tachyzoite/vacuole (<50 pix^3), 2 tachyzoites/vacuole (50<100 pix^3) or >4 tachyzoites/vacuole (>100 pix^3) at 6 and 24 hpi. Pooled data from 3 independent experiments with at least 3 larvae per time point. Mean ± SEM shown. (C) Representative AirScan confocal images of replicating tachyzoites

in larvae infected in the HBV with type I *Toxoplasma*-GFP (green; top left), fixed at 0, 6 and 24 hpi and labelled with α-GRA2 (red; top right) and merge (bottom large panel). Showing 1, 2 or >4 tachyzoites/vacuole. Scale bar, 2 μm.

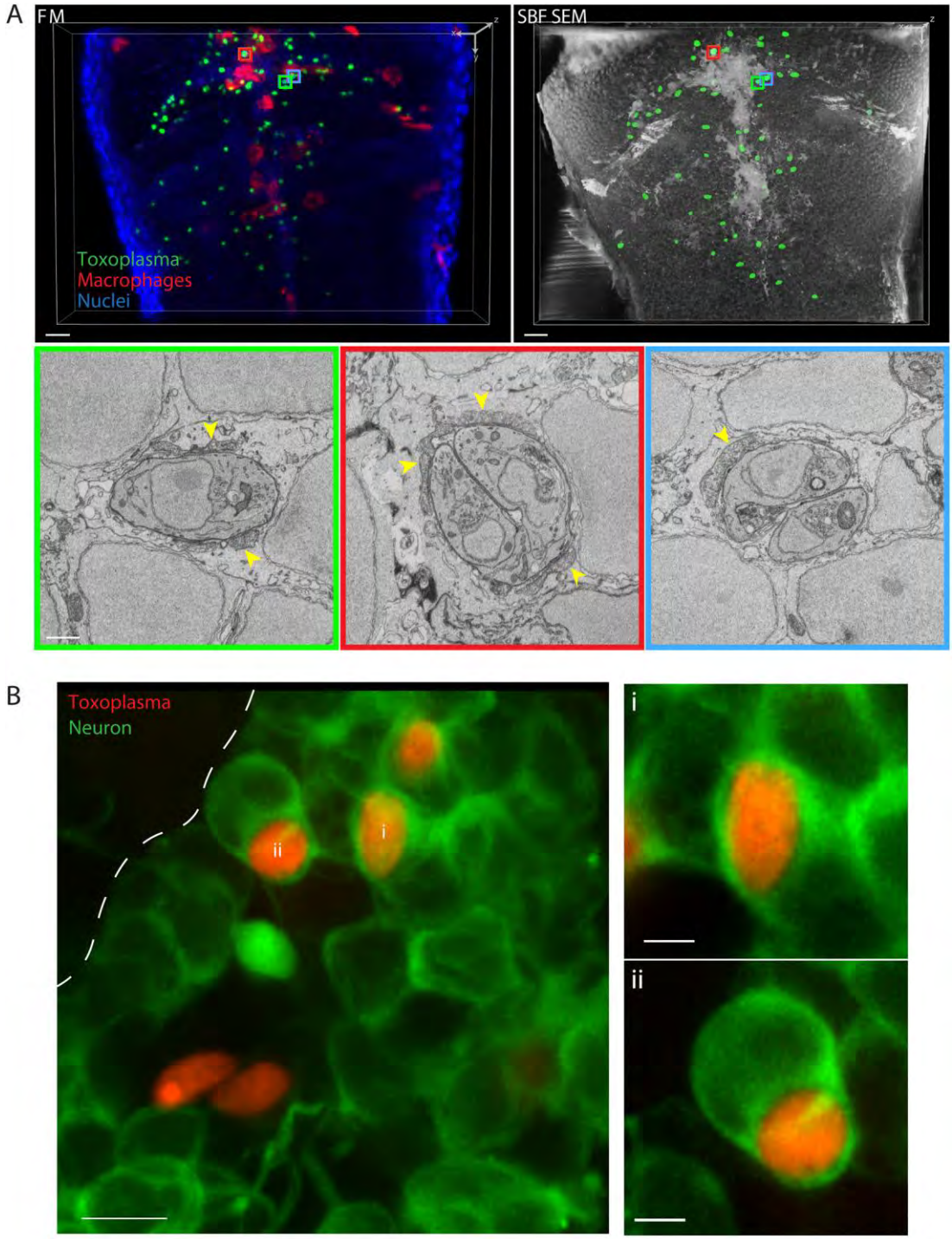

Figure 2. *Toxoplasma gondii* tachyzoites reside within zebrafish brain cells and neurons. (A) 3D CLEM of tachyzoites in the HBV of transgenic *mpeg1:G/U:*mCherry larvae harboring red macrophages infected with type I *Toxoplasma*-GFP (green) at 6 hpi. 3D reconstructions of 40 confocal Z-slices

of a full vibratome section (FM; fluorescence microscopy, top left panel) and of 354 inverted consecutive 50 nm SBF SEM slices of a segment of it (top right panel). A middle slice of each of the *Toxoplasma* visible in the SBF SEM dataset was manually segmented (green, top right panel) to aid correlation. Regions of interest showing the localization of the high-resolution SBF SEM images (lower panels) are denoted with color boxes. Single (left, green box), replicating (middle, red box) and doublet (right, blue box) tachyzoites in zebrafish host cells were observed. See also Movie 2. Showing three representative images out of 36 total *Toxoplasma* in zebrafish brain cells (see Fig. S2), tachyzoites were imaged in their whole volume to accurately determine their stage. Host mitochondrial recruitment to the parasitophorous vacuole indicated by yellow arrowheads. Scale bar, 10 μm (top panels) and 1 μm (lower panels). (B) Representative AiryScan confocal images of 3 dpf Tg*(elavl3:GCaMP6s)*^{if4} larvae (neurons marked in green) infected in the HBV with type I *Toxoplasma*-Tomato (red) at 4 hpi. Showing a maximum projection image 35 Z-slices (covering 5.98 μm) out of 85 slices imaged (left, five tachyzoites total imaged). Ventricular surface highlighted by white dashed line. Of the three tachyzoites found within green neurons from left panel, showing magnified maximum projection image of two tachyzoites covering 8 (i, top right) or 17 (ii, bottom right) Z-slices (Z=0.17 μm) out of 85 total. Scale bar, 5 μm (left panel) and 2 μm (right panels). Two out of the five tachyzoites imaged are not inside green neurons (left panel), and close to the ventricular surface where green neurons become sporadic (see Movie 3), which suggests active invasion of progenitors / ependymal cells.

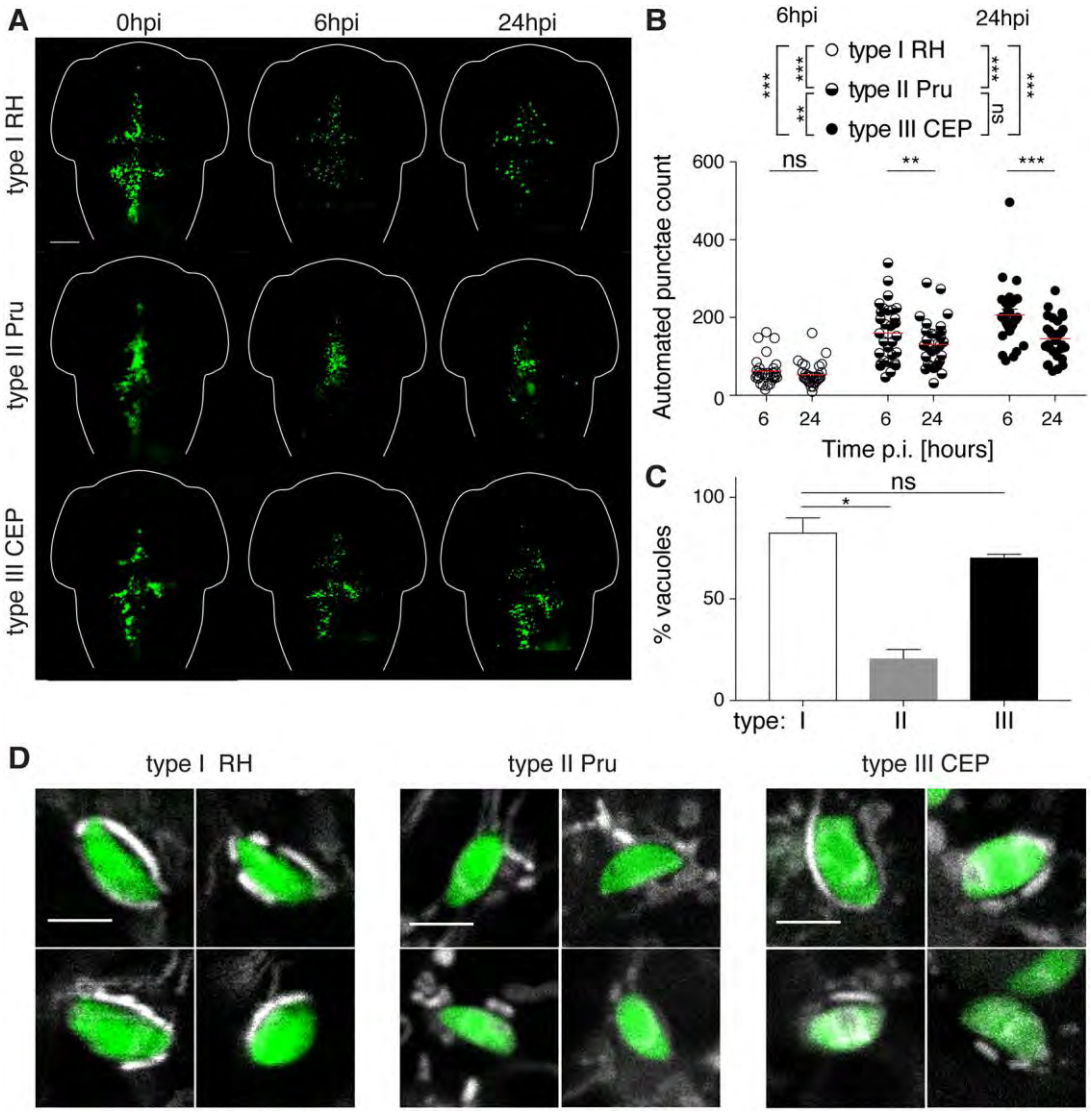

Figure 3. Non-lethal zebrafish larvae model of acute *Toxoplasma gondii* infection. (A) Representative images of larvae infected in the HBV with type I (RH, top panels), type II (Pru, middle panels) or type III (CEP, bottom panels) of *Toxoplasma* (green). Individual larvae were imaged and monitored at 0, 6 and 24 hpi (from left to right) by fluorescent stereomicroscopy. Scale bar, 100 μm. (B) Automated enumeration of GFP-positive punctae at 6 and 24 hpi of larvae infected with type I (RH, open circle), type II (Pru, semi-closed circle) or type III (CEP, closed circle) of *Toxoplasma* tachyzoites. Automated counts were supported by manual quantifications (Fig. S3C). Mean ± SEM shown.

Pooled data from at least 3 independent experiments with at least 5 larvae per condition per experiment. Significance calculated using 2-way ANOVA (repeated measures) with Sidak's multiple comparisons test, ns, $p>0.05$, **, $p\leq0.01$, ***, $p\leq0.001$. (C) Quantification of the percentage of type I (white bar), type II (grey bar) or type III (black bar) vacuoles exhibiting host mitochondrial association at 6hpi in the zebrafish hindbrain. Significant differences were observed between the parasite strains (Kruskal-Wallis $p = 0.0036$) with type II parasites shown to be lower (20 ± 4.3%) than type I (82 ± 7.2%) or type III (70 ± 1.6%). Significance calculated using Dunn's multiple comparisons test, ns, $p>0.05$, *, $p\leq0.05$. Pooled data from at least 3 independent experiments with 3 larvae per condition per experiment. Mean ± SEM shown. (D) Representative confocal images of larvae infected in the HBV with type I (RH, left panels), type II (Pru, middle panels) or type III (CEP, right panels) of *Toxoplasma* (green) and stained for mitochondria (white) 6 hpi. Showing four examples each of host mitochondrial recruitment (for type I and type III) or no host mitochondrial recruitment (for type II) Scale bar, 5 μm.

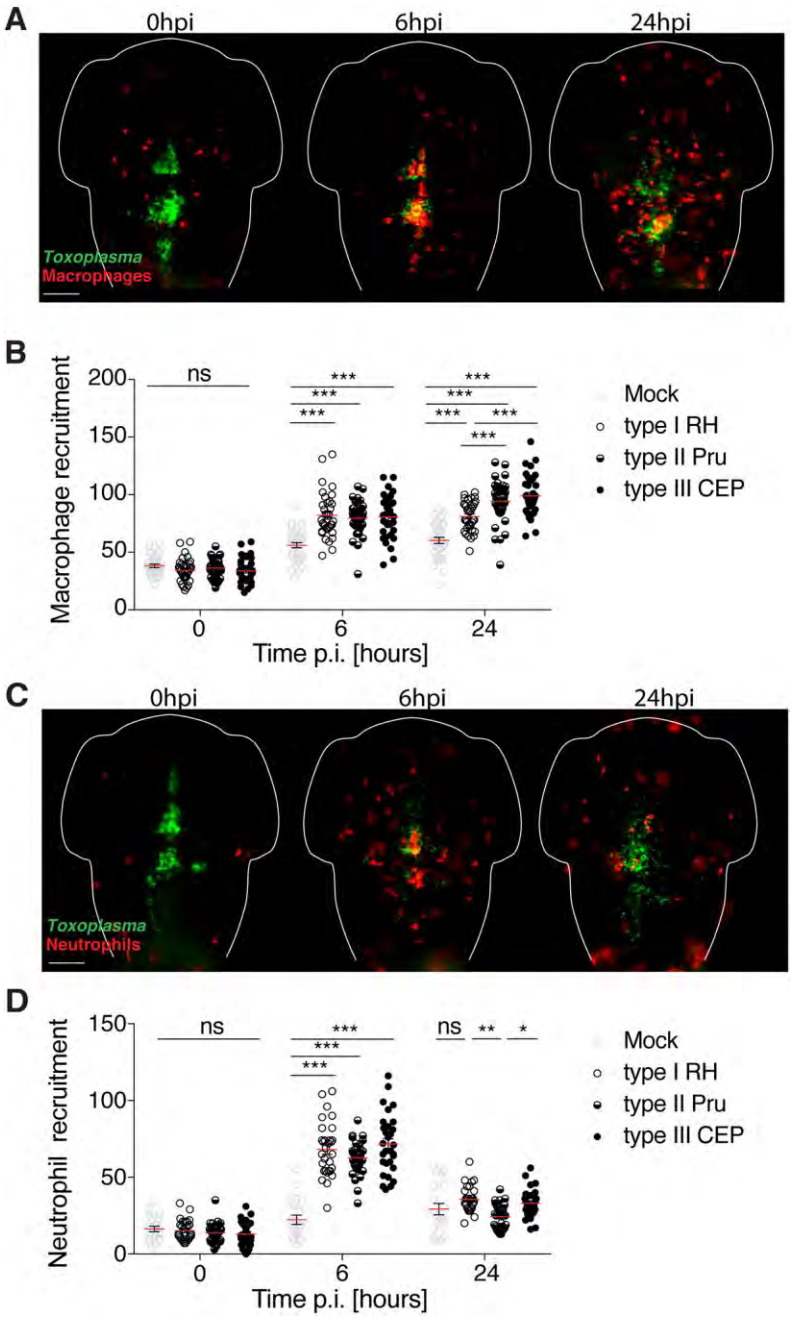

Figure 4. Leukocyte recruitment to *Toxoplasma gondii in vivo*. (A) Representative images of *mpeg1:G/U*:mCherry larvae harboring red macrophages infected in the HBV with *Toxoplasma* (green). Individual larvae were imaged and monitored at 0, 6 and 24 hpi (from left to right) by fluorescent stereomicroscopy. Scale bar, 100 μm. (B) Quantification of macrophages in *mpeg1:G/U*:mCherry larvae at 0, 6 and 24 hpi injected with

mock (HFF lysate, grey open circle), type I (RH, open circle), type II (Pru, semi-closed circle) or type III (CEP, closed circle). Pooled data from at least 3 independent experiments with at least 7 larvae per condition per experiment. Mean ± SEM shown. Significance calculated using 2-way ANOVA (repeated measures) with Sidak's multiple comparisons test, ns, $p>0.05$, ***, $p\leq0.001$. (C) Representative images of *lyz:*dsRed larvae harboring red neutrophils infected in the HBV with *Toxoplasma* (green). Individual larvae were imaged and monitored at 0, 6 and 24 hpi (from left to right) by fluorescent stereomicroscopy. Scale bar, 100 μm. (D) Quantification of neutrophils in *lyz:*dsRed larvae at 0, 6 and 24 hpi injected with mock (HFF lysate, grey open circle), type I (RH, open circle), type II (Pru, semi-closed circle) or type III (CEP, closed circle). Pooled data from at least 2 independent experiments with at least 3 larvae per condition per experiment. Mean ± SEM shown. Significance calculated using 2-way ANOVA (repeated measures) with Tukey's multiple comparisons test, ns, $p>0.05$, *, $p\leq0.01$, **, $p\leq0.01$, ***, $p\leq0.001$.

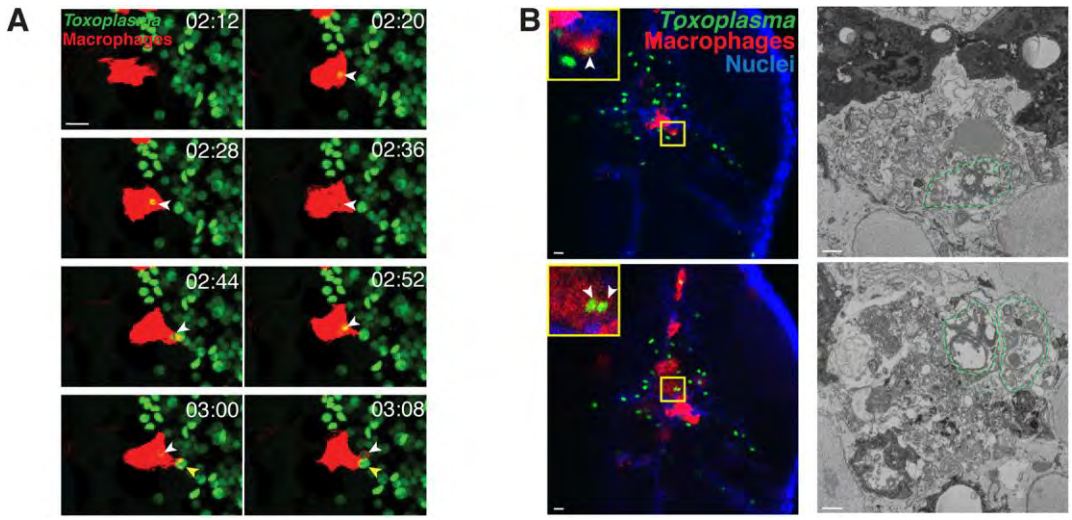

Figure 5. Macrophages phagocytose and degrade *Toxoplasma gondii in vivo*. (A) Representative frames extracted from *in vivo* confocal imaging of *mpeg1:G/U*:mCherry (red) larvae injected with type I *Toxoplasma*-GFP (green). First frame at 2 h 12 minutes post-infection (mpi) followed by seven consecutive frames taken at 8 minute intervals. Showing a maximum projection of 24 Z-slices taken at 2 μm optical sections. White arrowhead labels a phagocytosed parasite at 2 h 20 mpi that loses its green fluorescence by 3 h 8 mpi. Yellow arrowhead indicates a new phagocytosis event of a green parasite at 3 hpi to 3 h 8 mpi. Scale bar, 10 μm. See also Movie 5. (B) 3D CLEM of dead/dying tachyzoites in the HBV of *mpeg1:G/U:*mCherry (red) larvae infected with type I *Toxoplasma*-GFP (green) at 6 hpi and stained with Hoechst 33342 (blue). Representative images extracted from confocal z-stacks of a full vibratome section (left panel) and from consecutive 50 nm SBF SEM slices of a segment of it (right panel). Dead/dying parasites are indicated by white arrowheads (inset, left panels) and outlined by green dashed lines (right panels). Scale bar, 10 μm (left) and 1 μm (right).

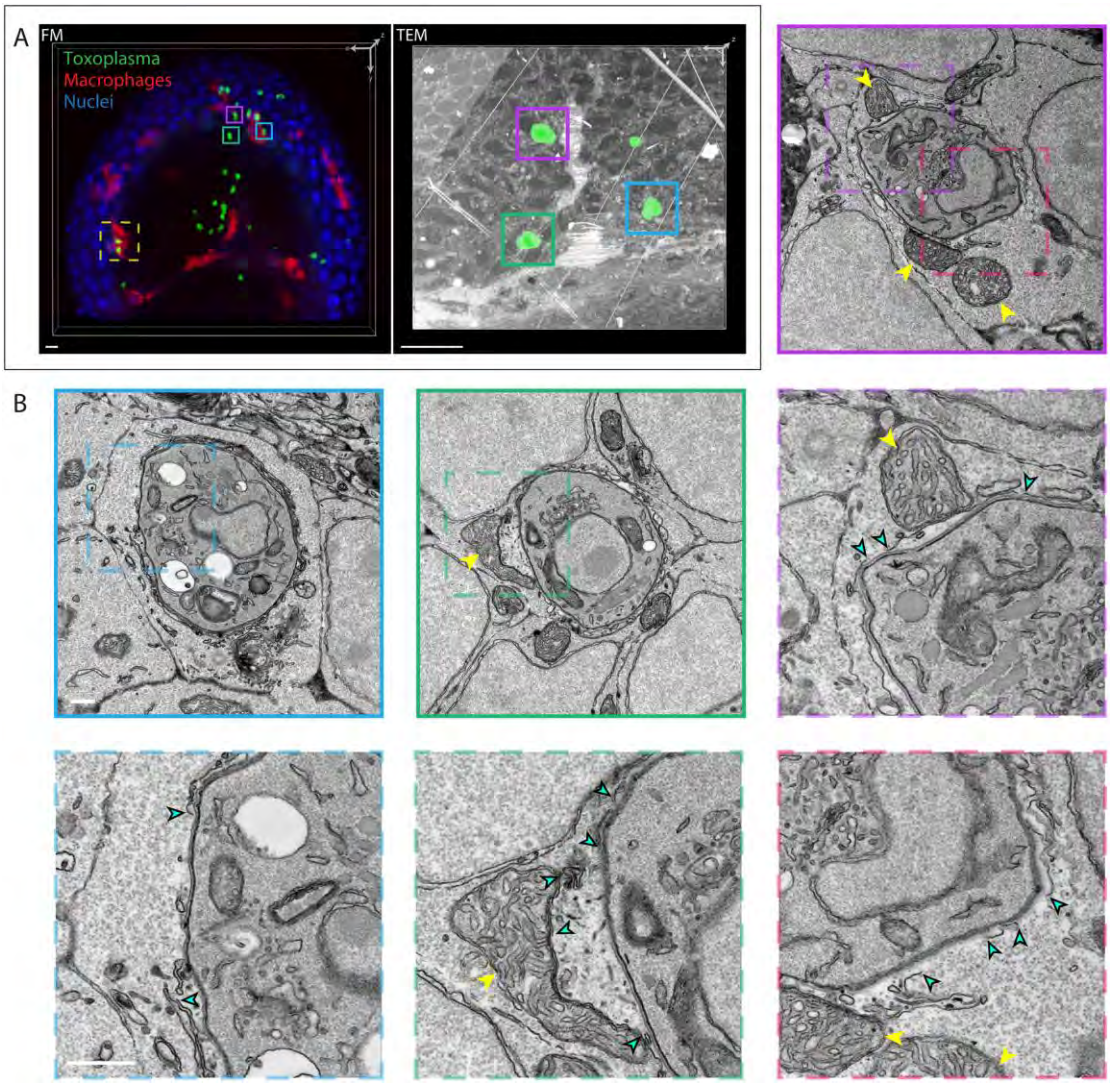

Figure 6. Host cell-intrinsic response in zebrafish disrupts *Toxoplasma gondii* parasitophorous vacuoles in brain cells *in vivo.* (A) 3D CLEM of tachyzoites in the HBV of transgenic *mpeg1:G/U:*mCherry larvae harboring red macrophages infected with type I *Toxoplasma*-GFP (green) at 6 hpi and stained with Hoechst 33342 (blue). 3D reconstructions of 59 confocal Z-slices (40x) of a part of the HBV (FM; fluorescence microscopy, left panel) and of 75 inverted consecutive 70 nm sections imaged by ssTEM at 440x magnification (top right panel). Each of the *Toxoplasma* visible in the ssTEM dataset was manually segmented (green, right panel) in every section to aid correlation.

Regions of interest showing the localization of the high-resolution ssTEM images shown in (B) (left- cyan box, middle- magenta box, right- green box) and Fig. 7 (yellow box) are denoted with color boxes. (B) Representative higher magnification ssTEM images of *Toxoplasma* in HBV cells. Continuous color boxes (top panels) show 6800x magnification images, dashed line boxes 18500x. *Toxoplasma* tachyzoites were imaged in their full volume to accurately assess the continuity of the PV. See also Movie 6. Host mitochondrial recruitment to the PV indicated by yellow arrowheads. Breaks in the PV indicated by cyan arrowheads. Scale bar, 10 μm (top panels) and 500 nm (lower panels).

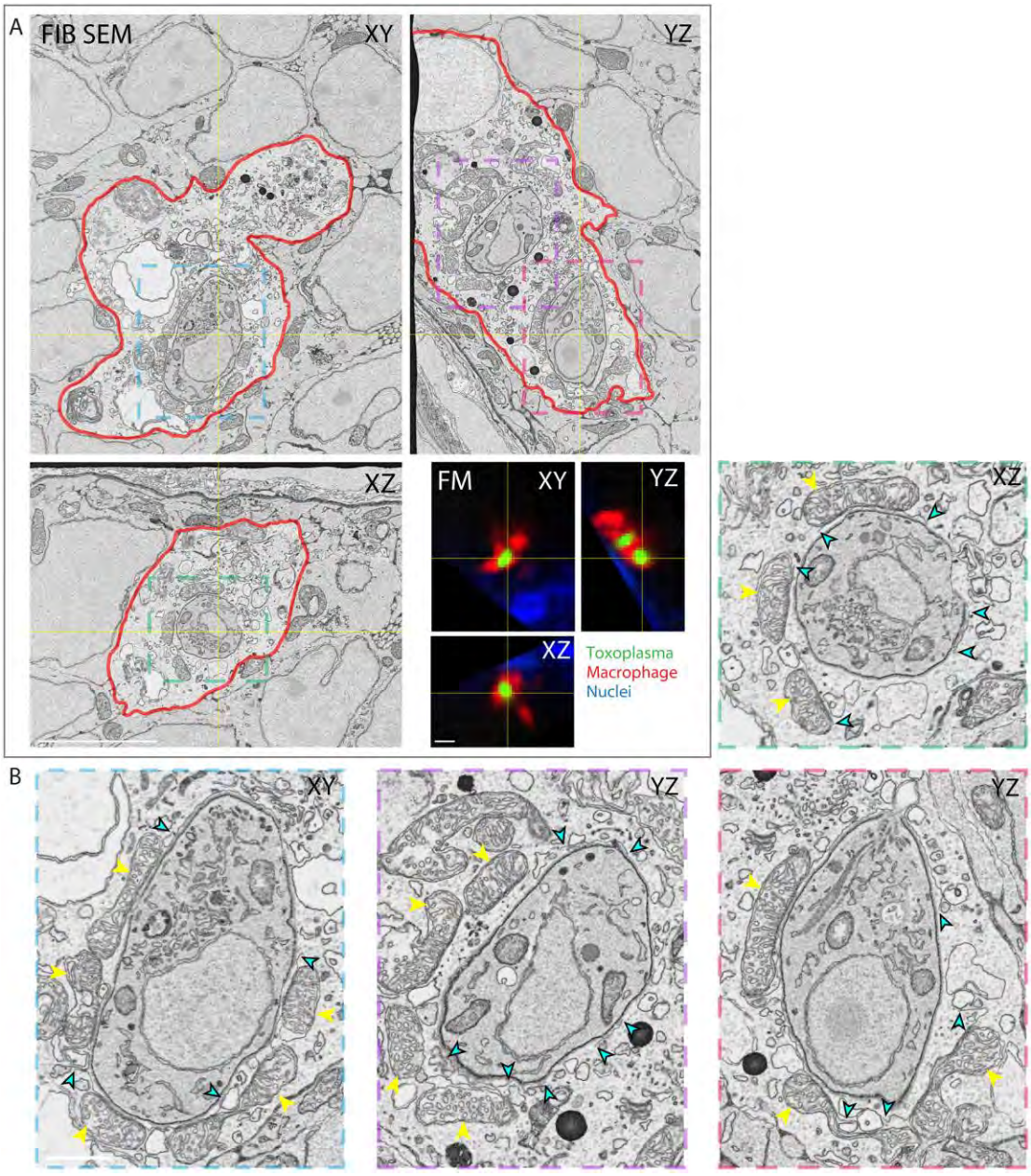

Figure 7. Host cell-intrinsic response disrupts *Toxoplasma gondii* parasitophorous vacuoles in zebrafish macrophages *in vivo.* (A) 3D CLEM of 2 parasites inside a macrophage in the HBV of *mpeg1:G/U*:mCherry (red) larvae infected with type I *Toxoplasma*-GFP (green) at 6 hpi and stained with Hoechst 33342 (blue). Orthoslices of 3200 consecutive 5 nm FIB SEM slices of the whole macrophage (top left panel- see also Movie 7) and of 59 confocal Z-slices (40x) re-sliced to match the orientation of the FIB SEM data

(FM, bottom right panel- cell also shown in yellow dashed line box in Fig. 6A). Color boxes show localization of the blow-ups shown in (B). The plasma membrane of the macrophage (red) was manually segmented to aid correlation. (B) Blow-ups of the *Toxoplasma* shown in the FIB SEM orthoslices in (A). Host mitochondrial recruitment to the PV indicated by yellow arrowheads, breaks in the PV by cyan arrowheads. Scale bar, 5 μm (top panels) and 1 μm (lower panels).

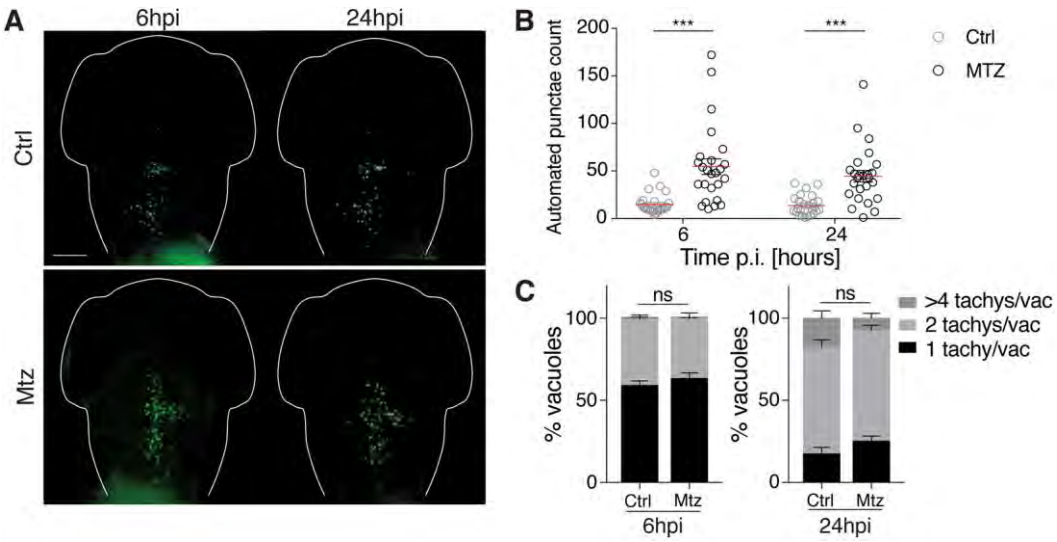

Figure 8. Macrophages control *Toxoplasma gondii* burden *in vivo*. (A) Representative images of control (Ctrl; top panels) or macrophage-ablated (Mtz; bottom panels) *mpeg:G/U:*mCherry larvae infected in HBV with type I *Toxoplasma*-GFP (green). Individual larvae were imaged at 6 and 24 hpi (from left to right) by fluorescent stereomicroscopy. Scale bar, 100 μm. (B) Automated enumeration of GFP-positive punctae in the HBV at 6 and 24 hpi of Ctrl (open circle) or macrophage-ablated (closed circle) larvae infected with type I *Toxoplasma* tachyzoites. Pooled data from 3 independent experiments with at least 7 larvae per condition per experiment. Significance calculated using 2-way ANOVA (repeated measures) with Sidak's multiple comparisons test, p≤0.001. (C) Pixel volume quantification of individual GFP-positive punctae in Ctrl or macrophage-ablated larvae at 6 and 24 hpi. Presented as percentage of total vacuoles counted in the HBV that are 1 tachyzoite/vacuole (<50 pix^3), 2 tachyzoites/vacuole (50<100 pix^3) or >4 tachyzoites/vacuole (>100 pix^3). Pooled data from 3 independent experiments with at least 3 larvae per time point. Significance calculated using Chi-square test, X^2_2 = 1.248 (6 hpi), X^2_2 = 5.4 (24 hpi), p>0.05. Mean ± SEM shown.

Supplementary Information

Supplementary Figure 1.

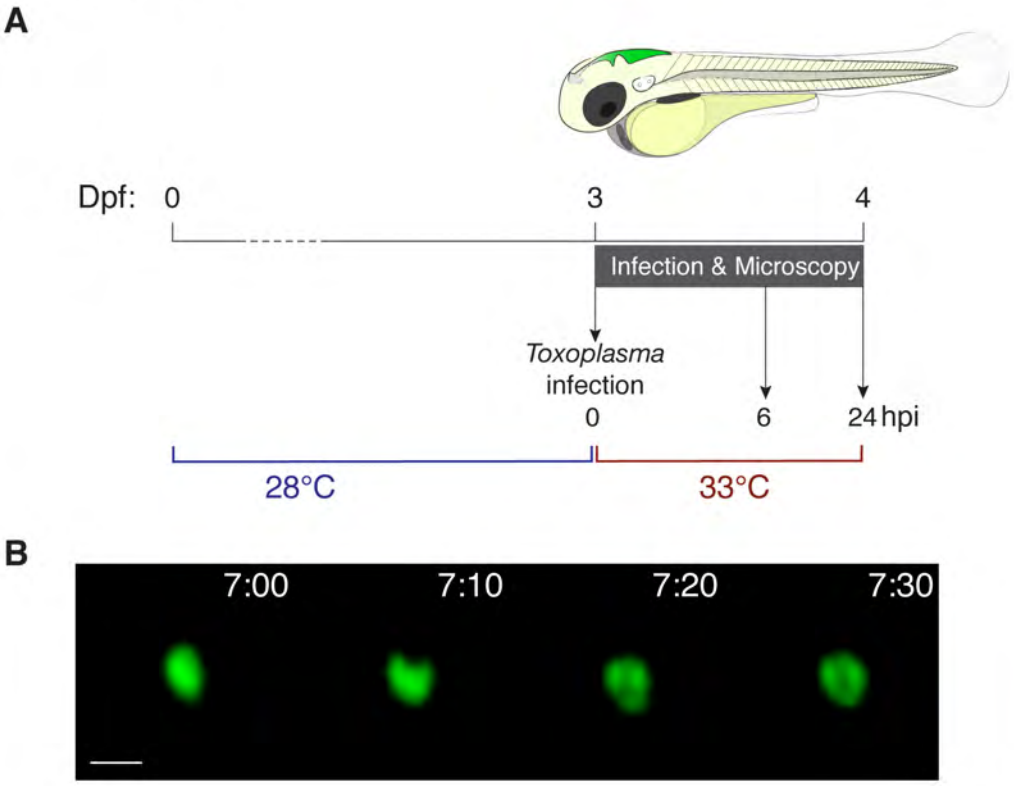

Figure S1. *Toxoplasma gondii* tachyzoites are intracellular and replicate in zebrafish, related to Figure 1. (A) Schematic of the infection model utilized with a cartoon of the zebrafish larva (3 dpf) highlighting the site of *Toxoplasma* tachyzoite injection in the hindbrain ventricle (HBV) in green. Infected larvae were maintained at 33°C post-injection and monitored up to 24 hours post-infection (hpi). (B) Representative frames extracted from *in vivo* widefield imaging of larvae injected with type I *Toxoplasma*-GFP (green). First frame at 7 hpi followed by three consecutive frames taken at 10 minute intervals. Showing a single Z-plane from 60 taken at 2 µm optical sections. Scale bar, 5 µm. See also Movie 1.

Supplementary Figure 2.

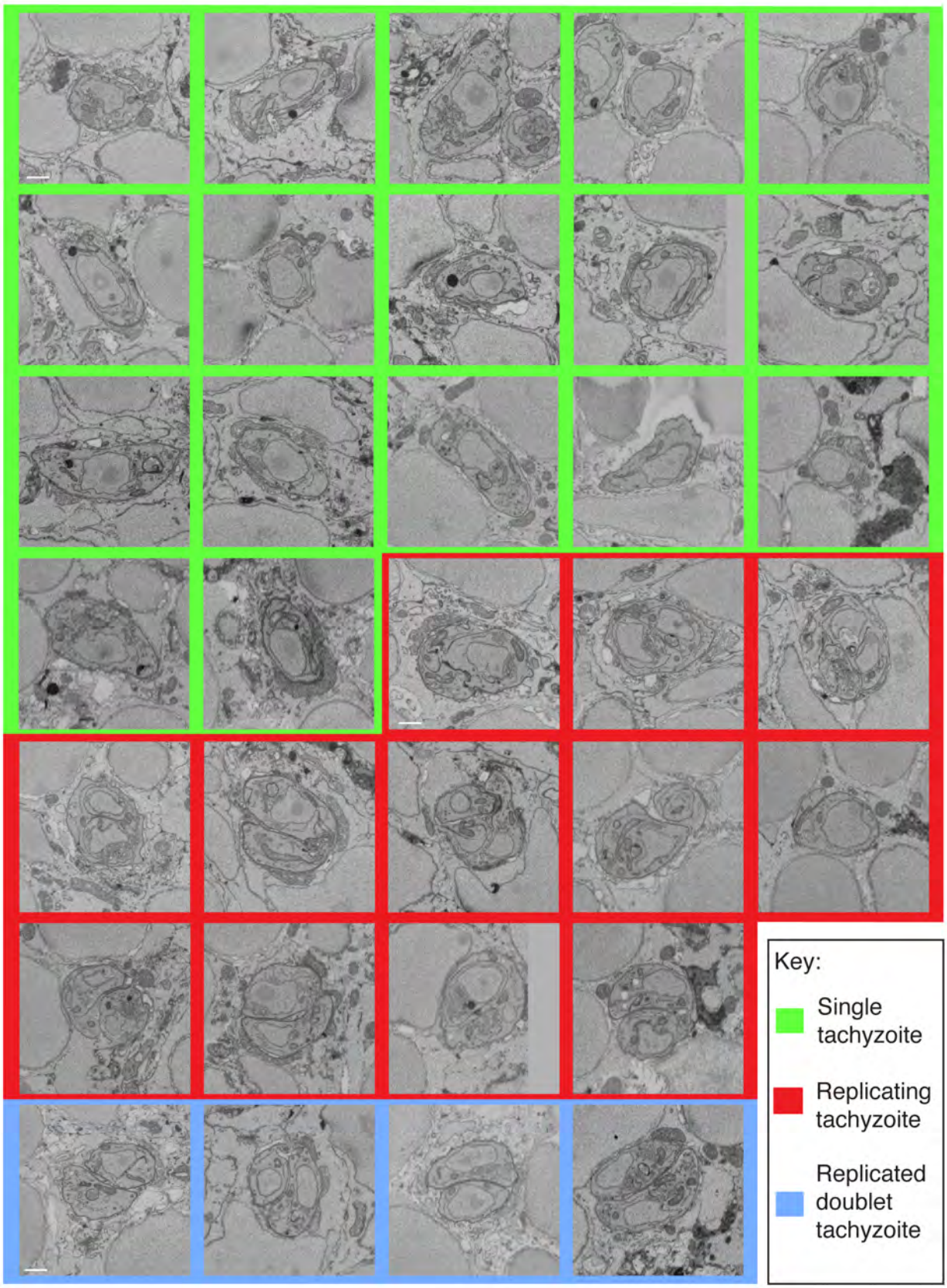

Figure S2. 3D CLEM of single, replicating and doublet tachyzoites in the zebrafish hindbrain, related to Figure 2. 3D CLEM of tachyzoites in the HBV of *mpeg1:G:U:*mCherry larvae infected with type I *Toxoplasma*-GFP at 6 hpi. Representative images of 33/36 *Toxoplasma* in zebrafish host cells extracted from stacks of consecutive 50 nm SBF SEM slices. *Toxoplasma* tachyzoites were imaged in their full volume to accurately determine their replicative stage. Single (green box), replicating (red box) and replicated doublet (blue box) tachyzoites were observed. Scale bar, 1 µm.

Supplementary Figure 3.

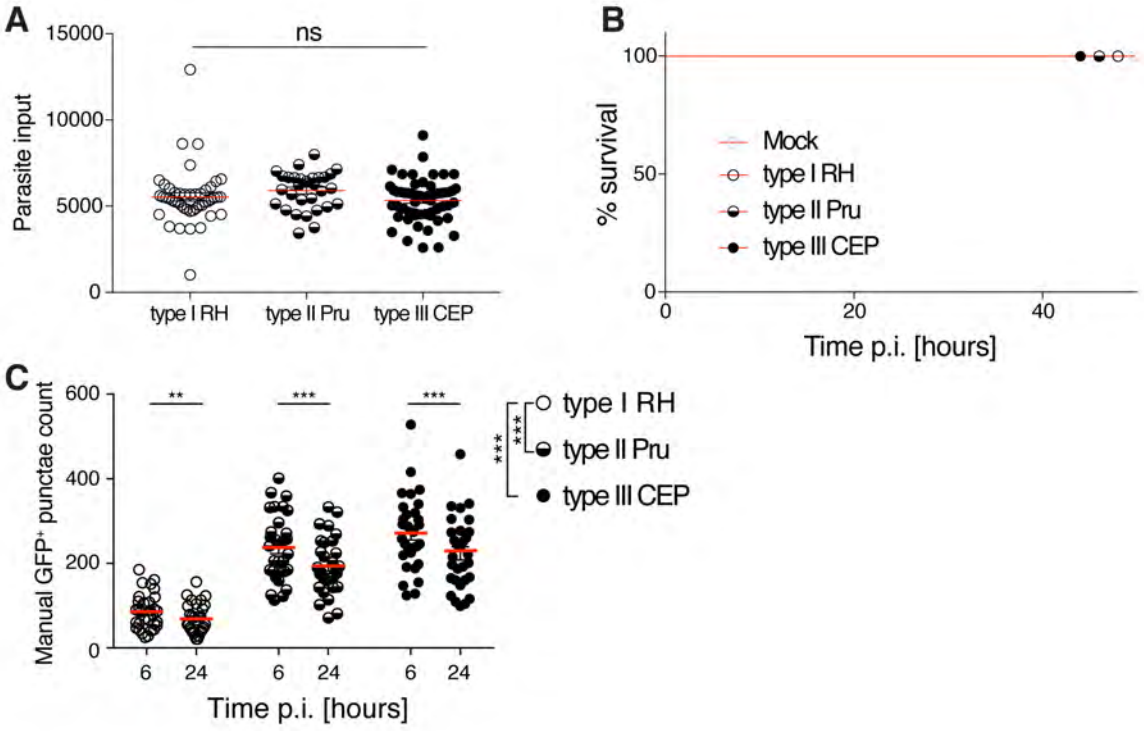

Figure S3. The zebrafish larvae model of acute *Toxoplasma gondii* infection is non-lethal, related to Figure 3. (A) Quantification of type I (RH, open circle), type II (Pru, semi-closed circle) or type III (CEP, closed circle) input dose of *Toxoplasma*-GFP using particle analysis of infected HBV images obtained by fluorescent stereomicroscopy at 0 hpi. Mean ± SEM shown. Significance calculated using one-way ANOVA with Tukey's multiple comparisons test, ns, $p>0.05$. (B) Survival curves of larvae injected with mock (human foreskin fibroblast lysate), type I (RH), type II (Pru) or type III (CEP) *Toxoplasma* tachyzoites. Pooled data from at least 3 independent experiments with at least 5 larvae per condition per experiment. (C) Manual enumeration of GFP-positive punctae in the HBV at 6 and 24 hpi of type I (RH, open circle), type II (Pru, semi-closed circle) or type III (CEP, closed circle) *Toxoplasma*-GFP. Mean ± SEM shown. Pooled data from at least 3 independent experiments with at least 5 larvae per condition per experiment. Significance calculated using 2-way ANOVA (repeated measures) with Sidak's multiple comparisons test, **, $p\leq0.01$, ***, $p\leq0.001$.

Supplementary Figure 4.

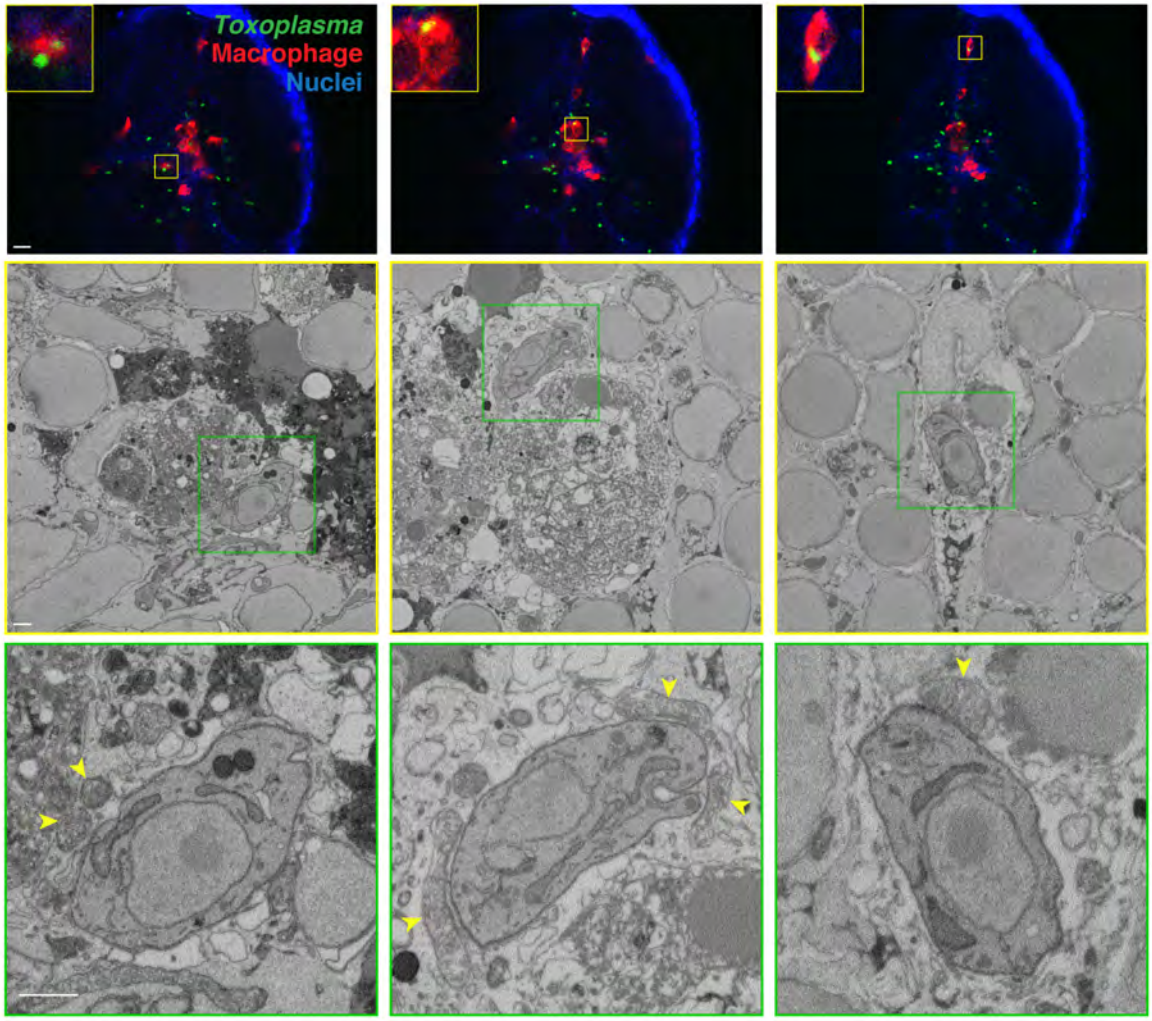

Figure S4. *Toxoplasma gondii* actively invade zebrafish macrophages. 3D CLEM of parasites inside macrophages in the HBV of *mpeg1:G/U:*mCherry (red) larvae infected with type I *Toxoplasma-GFP* (green) at 6 hpi stained with Hoechst 33342 (blue). Representative images extracted from 44 confocal Z-slices of a full section (top panels). The localizations of respective high-resolution SBF SEM images (middle panels) are denoted with yellow boxes. The localization of respective enlarged high-resolution SBF SEM images (bottom panels) of *Toxoplasma* are denoted with green boxes. Host mitochondrial recruitment to the parasitophorous vacuole indicated by yellow arrowheads. Scale bars, 20 µm (top panels) and 1 µm (middle and bottom panels).

Supplementary Figure 5.

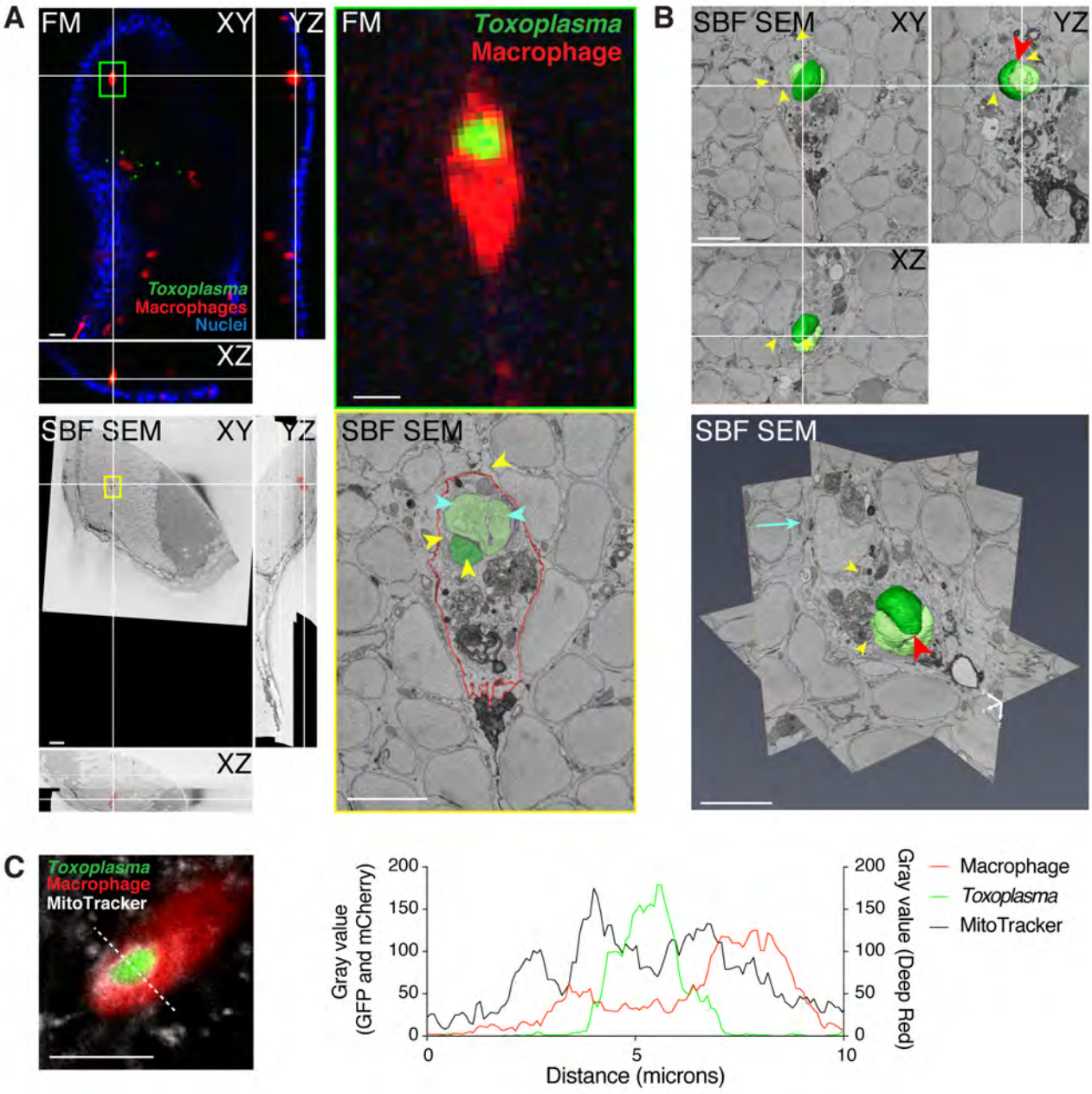

Figure S5. Replicative *Toxoplasma gondii* inside a zebrafish macrophage. (A) 3D CLEM of parasite replication inside a macrophage in the HBV of *mpeg1:G/U*:mCherry (red) larvae infected with type I *Toxoplasma*-GFP (green) at 6 hpi and stained with Hoechst 33342 (blue). Orthoslices of 44 confocal Z- slices of a full vibratome section (FM, left top panel) and of 1662 consecutive 50 nm SBF SEM slices from a subregion of it (left bottom panel). Color boxes show localization of the confocal (right top, green) and high-resolution SBF SEM images (right bottom, yellow). The two replicating *Toxoplasma* (green and light green) and plasma membrane of the macrophage (red) were manually segmented. Blue arrowheads in the light green *Toxoplasma* indicates two nuclei. Host mitochondrial recruitment to the PV indicated by yellow arrowheads. Scale bars, 20 µm (left) and 5 µm (right). (B) Orthoslices (top panel) and 3D view (bottom panel) of the 3D model of the two segmented type I *Toxoplasma* shown in (A) overlaid on 373 consecutive 50 nm SBF SEM slices. Area where the two *Toxoplasma* are still joined indicated by the red arrowhead, nucleus of the macrophage by the blue arrow, host mitochondrial recruitment to the PV by yellow arrowheads. Scale bars, 5 µm. See also Movie 4. (C) Representative image extracted from a Z-stack from confocal imaging of live *mpeg1:G/U:*mCherry (red) larvae infected in the HBV with type I *Toxoplasma*-GFP (green) and stained with MitoTracker (grey) at 6 hpi and the fluorescent intensity profile of a parasite exhibiting host mitochondrial association within a macrophage. Image was smoothened post-acquisition by applying gaussian blur 0.75 pixel radius. Scale bar, 10 µm.

Supplementary Figure 6.

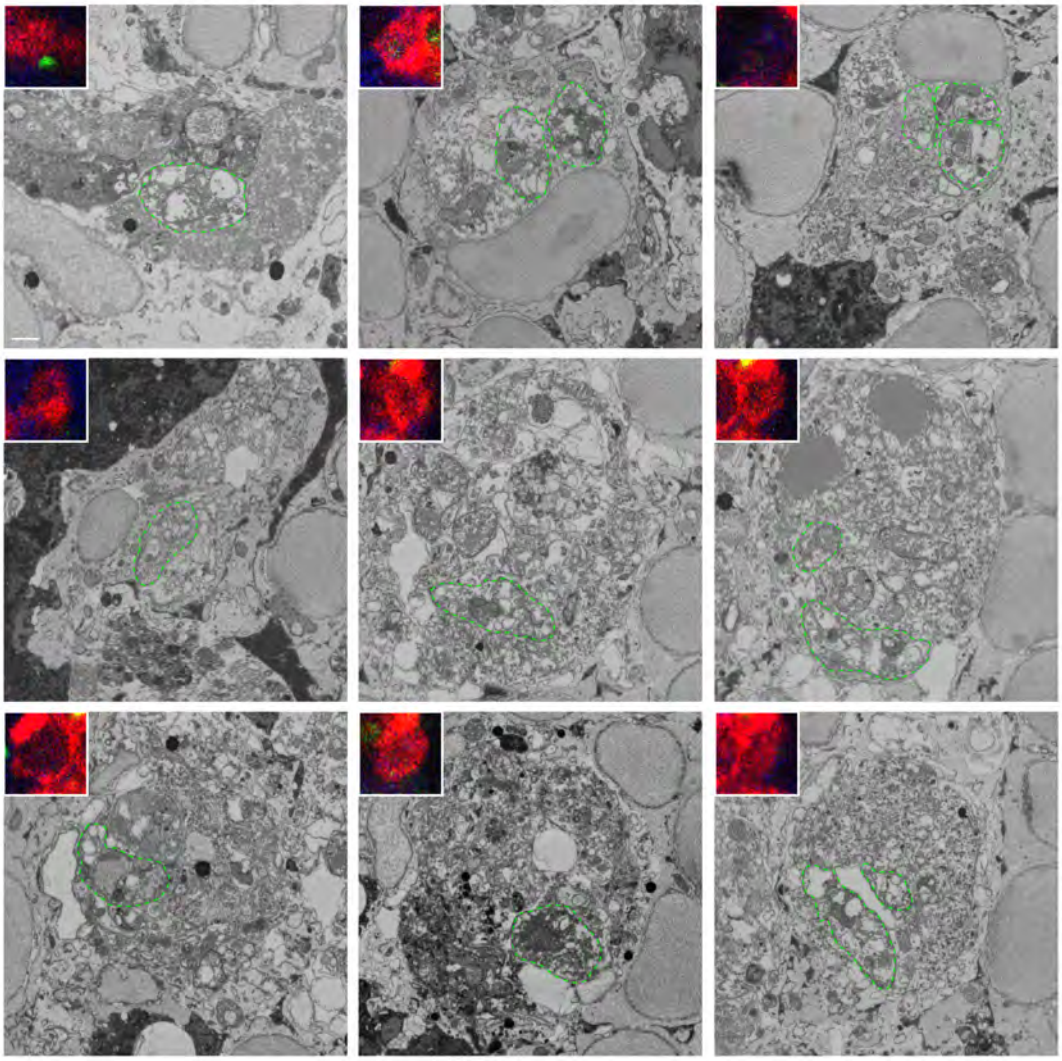

Figure S6. *Toxoplasma gondii* is degraded upon phagocytosis by zebrafish macrophages, related to Figure 5. 3D CLEM of putative dead tachyzoites in the HBV of *mpeg1:G/U:*mCherry (red) larvae infected with type I *Toxoplasma*-GFP (green) at 6 hpi and stained with Hoechst 33342 (blue). Representative images extracted from confocal Z-stacks of a full section (inset) and from Z-stacks of 50 nm SBF SEM slices of a segment of it. Only the first parasite (top left) showed GFP fluorescence. Putative dead parasites indicated by green dashed outline. Scale bar, 1 µm.

Supplementary Figure 7.

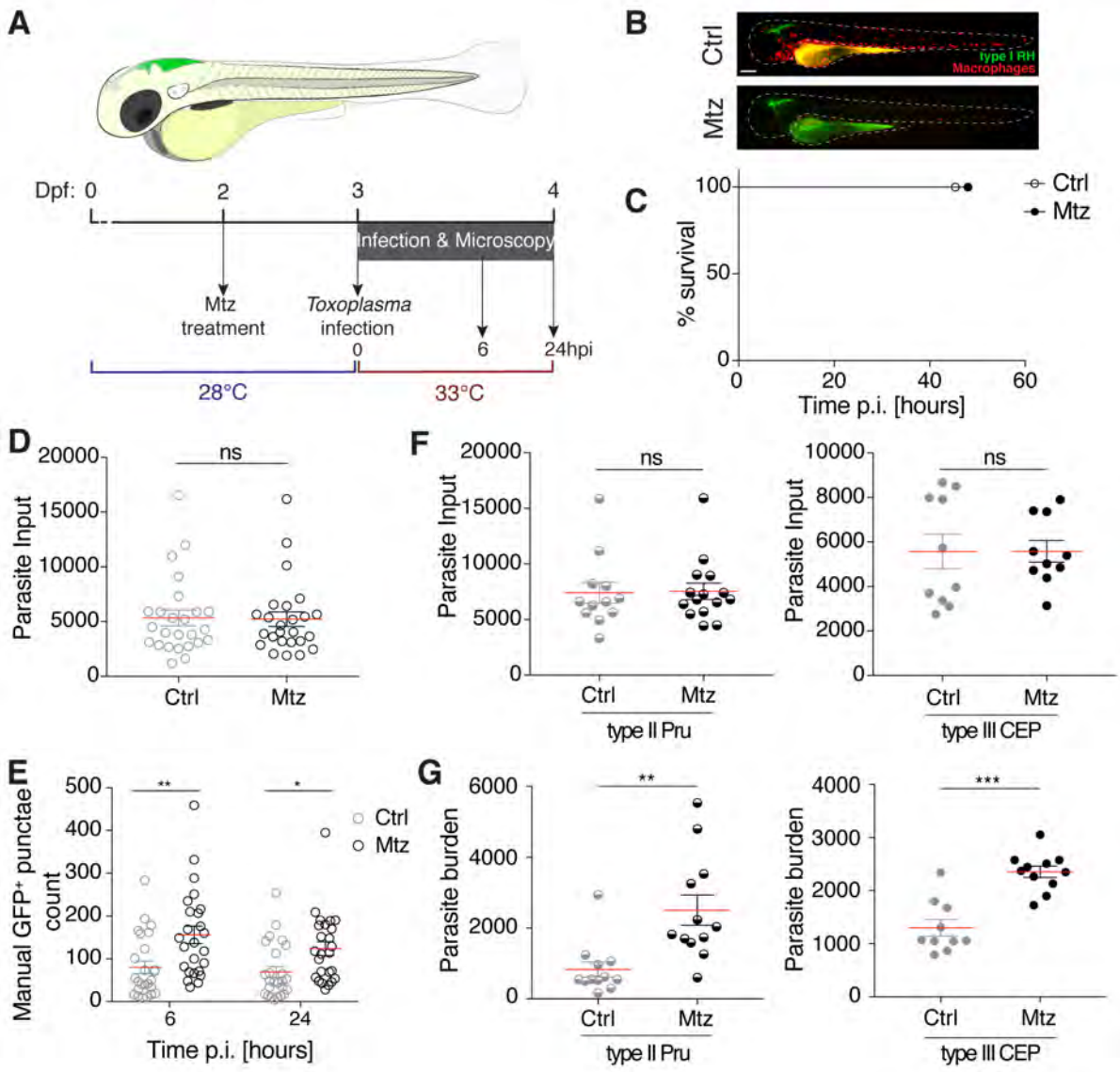

Figure S7. *Toxoplasma gondii* is controlled by zebrafish macrophages, related to Figure 8. (A) Schematic of the infection model utilized with a cartoon of the zebrafish larva (3 dpf) highlighting the site of *Toxoplasma* tachyzoite injection in the HBV in green. Prior to infection, larvae were pre-treated from 2 dpf with DMSO (control, Ctrl) or metronidazole (Mtz). Infected larvae were maintained at 33°C post-infection and monitored up to 24 hpi. (B) Representative images of Ctrl or Mtz treated *mpeg1:G/U:*mCherry larvae (red) injected with type I *Toxoplasma*-GFP (green) at 0 hpi. Scale bar, 200 µm. (C) Survival curves of Ctrl (open circles) or macrophage-ablated (Mtz-treated *mpeg1:G/U:*mCherry, closed circles) larvae infected in the HBV with type I *Toxoplasma*-GFP. Pooled data from 3 independent experiments with at least 7 larvae per condition per experiment. (D) Quantification of input dose of type I *Toxoplasma*-GFP in Ctrl (grey, open circle) or macrophage-ablated (Mtz; black, open circle) larvae using particle analysis of infected HBV images obtained by fluorescent stereomicroscopy at 0 hpi. Mean ± SEM shown. Significance calculated using unpaired t-test, ns, $p>0.05$. (E) Manual enumeration GFP-positive punctae in the HBV at 6 and 24 hpi of Ctrl (grey) or macrophage-ablated (Mtz; black) larvae infected with type I *Toxoplasma*-GFP. Mean ± SEM shown. Pooled data from 3 independent experiments with at least 7 larvae per condition per experiment. Significance calculated using 2-way ANOVA (repeated measures) with Sidak's multiple comparisons test, *, $p\leq0.05$, **, $p\leq0.01$. (F) Quantification of input dose of type II (semi-closed circle, left graph) or type III (closed circle, right graph) *Toxoplasma*-GFP in Ctrl (grey) or macrophage-ablated (Mtz; black) larvae using particle analysis of

infected HBV images obtained by fluorescent stereomicroscopy at 0 hpi. Mean ± SEM shown. Significance calculated using unpaired t-test, ns, $p>0.05$. (G) Quantification of parasite burden in the HBV of Ctrl (grey) or macrophage-ablated (Mtz; black) larvae infected with type II (semi-closed circle, left graph) or III (closed circle, right graph) at 24 hpi. Mean ± SEM shown. Showing 1 representative experiment of 3 with at least 10 larvae per condition per experiment. Significance calculated using unpaired t-test, **, $p\leq0.01$, ***, $p\leq0.001$.

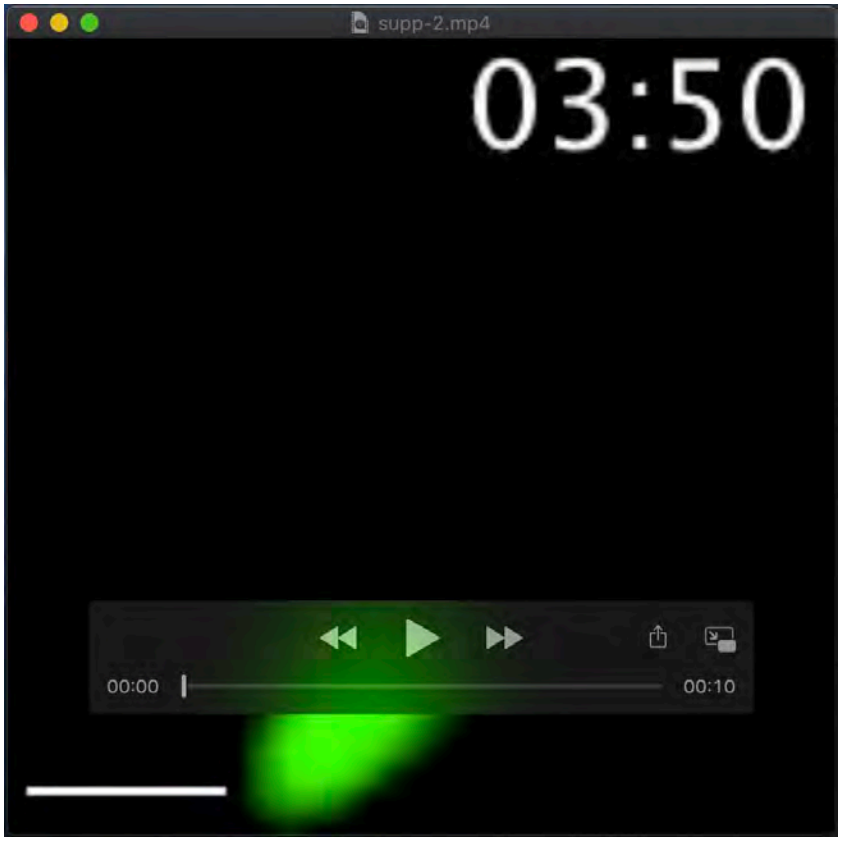

Movie 1. *In vivo* replication of *Toxoplasma gondii*, related to Figure S1B.

In vivo fluorescent widefield imaging of zebrafish larvae injected with type I *Toxoplasma*-GFP (green). First frame at 3 h 50 minutes post-infection (mpi) followed by frames taken at 10 minute intervals until 8 h 30 mpi. Showing a single Z-plane from 60 taken at 2 µm optical section. Scale bar, 5 µm.

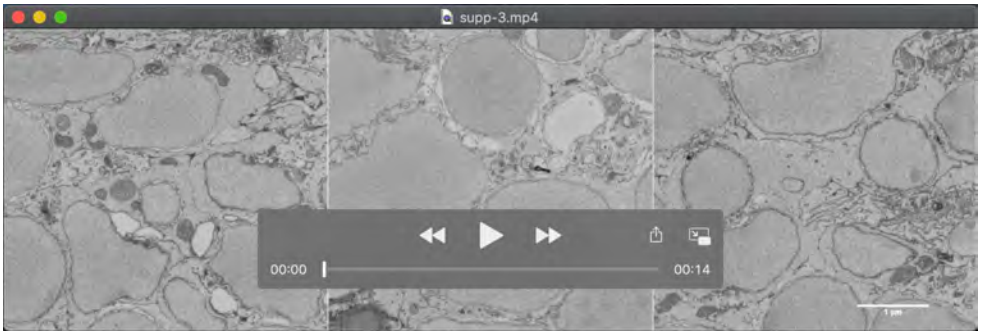

Movie 2. 3D CLEM of *Toxoplasma gondii* replication in the zebrafish hindbrain, related to Figure 2A. SBF SEM of tachyzoites in the HBV of larvae injected with type I *Toxoplasma*-GFP at 6 hpi. Representative examples of single (left), replicating (middle) and replicated doublet (right) *Toxoplasma* from a total of 36 found in zebrafish cells and imaged in their full volume to accurately determine their stage (see Fig. 2A and Fig. S2). 112 consecutive 50 nm SBF SEM slices of a different subregion of a section for each example. Scale bar, 1 µm.

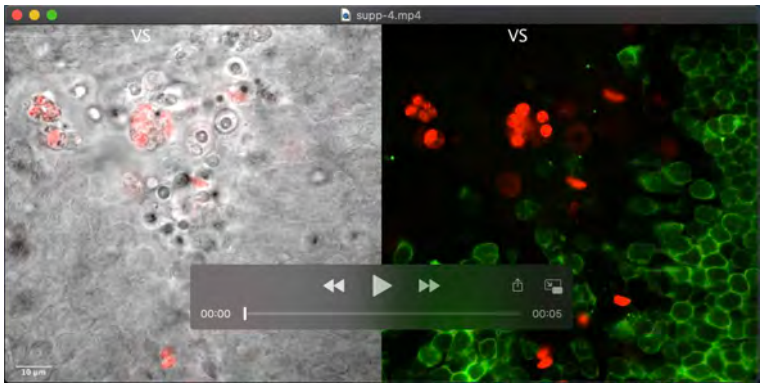

Movie 3. *Toxoplasma* tachyzoites reside within neurons, related to Figure 2B. *In vivo* confocal microscopy imaging of live 3 dpf Tg*(elavl3:GCaMP6s)*^{jf4} larvae (neurons marked in green) infected in the HBV with type I *Toxoplasma*-Tomato (red) at 4 hpi. A Z-stack of 33 Z-slices (Z=0.43 µm) is shown at 6 fps showing brightfield (grey) and *Toxoplasma* (red) composite (left) or *Toxoplasma* (red) and neurons (green) composite (right). Ventricular surface labeled as VS. The five tachyzoites shown in Fig. 2B are labeled with white arrowheads. Scale bar, 10 µm.

Movie 4. 3D CLEM of replicative *Toxoplasma gondii* inside a zebrafish macrophage, related to Figure S5B. SBF SEM of intraphagocytic parasite replication in the HBV of *mpeg1*:G/U:mCherry larvae infected with type I *Toxoplasma*-GFP at 6 hpi. 373 consecutive 50 nm SBF SEM slices in which the replicating *Toxoplasma* (green and light green) and plasma membrane of the macrophage (red) were manually segmented. A surface was generated to build a 3D model of the 2 segmented *Toxoplasma* in Amira software. Scale bar, as indicated.

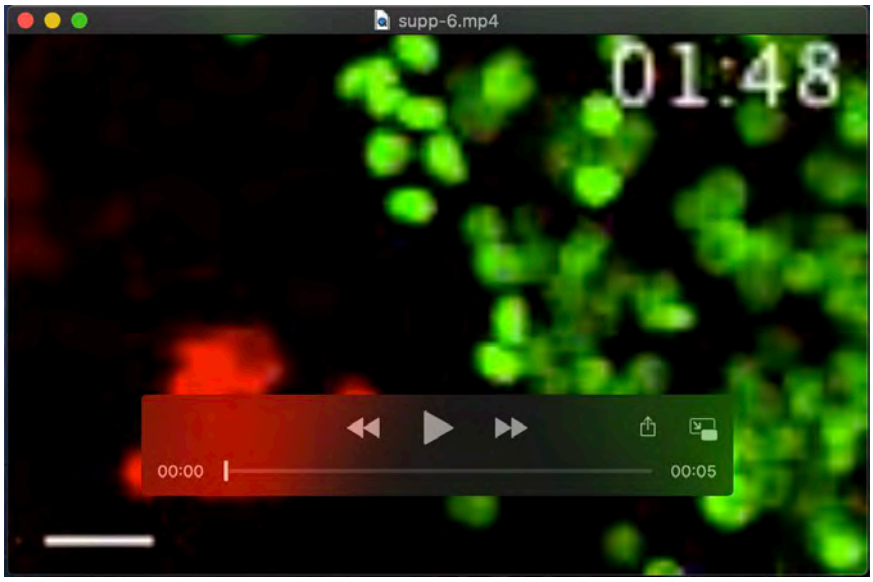

Movie 5. Phagocytosis of *Toxoplasma gondii* by a macrophage, related to Figure 5A. *In vivo* confocal imaging of *mpeg1*:G/U:mCherry larvae harboring red macrophages injected with type I *Toxoplasma*-GFP (green). First frame at 1 h 48 mpi followed by frames taken at 8 minute intervals until 3 h 48 mpi. Showing a maximum projection of 24 Z-slices from 60 taken at 2 µm optical sections. Scale bar, 10 µm.

Movie 6. Host cell-intrinsic response disrupts *Toxoplasma* parasitophorous vacuoles in zebrafish brain cells *in vivo*, related to Figure 6. ssTEM of parasite replication in brain cells in the HBV of *mpeg1*:G/U:mCherry larvae infected with type I *Toxoplasma*-GFP at 6 hpi. Movie shows 71 consecutive 70 nm sections imaged by ssTEM at 6800x magnification at 3 fps. *Toxoplasma* tachyzoites were imaged in their full volume to accurately assess the continuity of the PV. Color boxes (left- cyan box, middle- magenta box, right- green box) match the ones in Fig. 6. Scale bar, 1 µm.

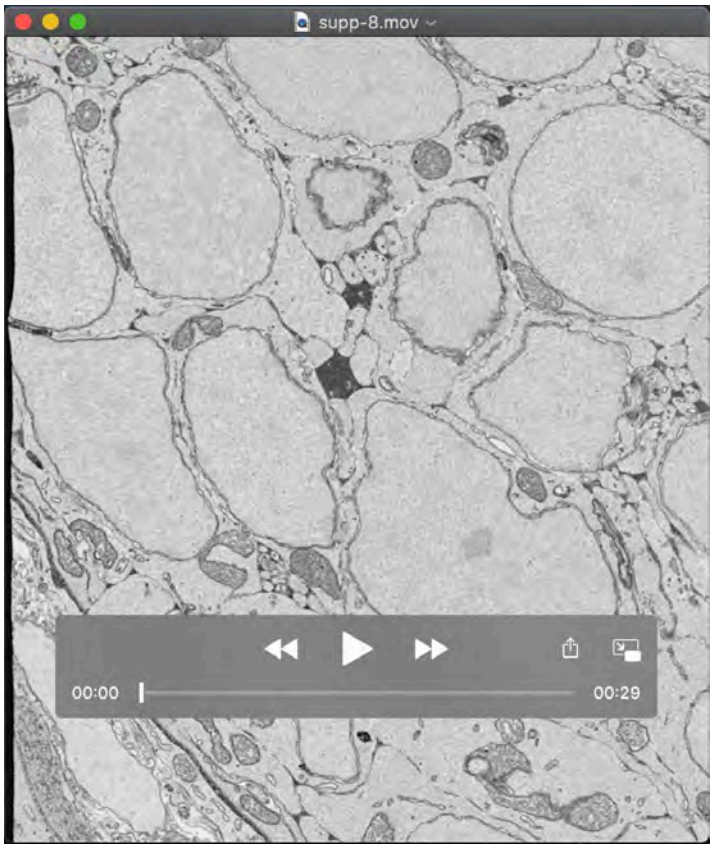

Movie 7. Host cell-intrinsic response disrupts *Toxoplasma* parasitophorous vacuoles in zebrafish macrophages *in vivo*, related to Figure 7. FIB SEM of two parasites inside a macrophage in the HBV of *mpeg1:G/U*:mCherry larvae infected with type I *Toxoplasma*-GFP at 6 hpi. The data was binned to 20 nm^3 to fit within the size constraints. Movie shows 860 consecutive slices through the YZ axis, as shown in Fig. 7. Scale bar, 5 µm (top panels) and 1 µm (lower panels). Field of view of 16 x 19 µm in XY.

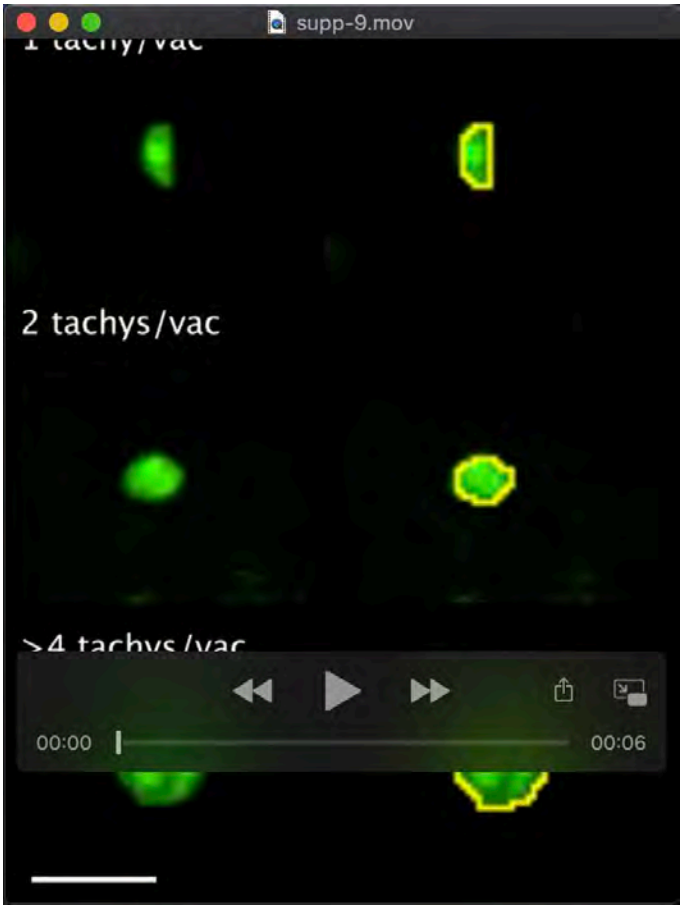

Movie 8. 3D visualization of *Toxoplasma gondii* replication in the zebrafish hindbrain by confocal microscopy for pixel volume analysis. Showing representative 3D reconstruction of confocal images of GFP-positive replicating tachyzoites in fixed zebrafish larvae infected with type I *Toxoplasma*-GFP (green). Volumes were categorized into 1 tachyzoite/vacuole (<50 pix^3, top), 2 tachyzoites/vacuole (50<100 pix^3, middle) or >4 tachyzoites/vacuole (>100 pix^3, bottom). Outline of GFP-positive punctae volumes measured is in yellow (left). Scale bar, 10 µm.